Journal of Sound and Vibration 529 (2022) 116850

Contents lists available at ScienceDirect

Journal of Sound and Vibration

journal homepage: www.elsevier.com/locate/jsvi

Interval-based identification of response-critical joints: A tool for model refinement

J.W.R. Meggitt

Acoustics Research Centre, University of Salford, Greater Manchester, M5 4WT, United Kingdom

ARTICLE INFO

Keywords:
Joint dynamics
Interval analysis
Sensitivity analysis
Possibilistic
Model refinement

ABSTRACT

To accurately model the dynamics of a complex built-up structure it is often necessary to forgo the assumption of ideal rigid coupling between components. The dynamic behaviour of inter-component connections, or joints, can have a significant impact on the performance, even survivability, of an assembled structure. For complex structures, where many joints are present, the complete characterisation and/or modelling of all joints is often not feasible. Hence, in the development or refinement of a component-based model there is a need to identify the *response-critical joints* of an assembly — those joints whose refinement would benefit the modelling effort most. In the present paper we address this issue by considering a 'possibilistic' interval-based assessment of joint variability, and propose a sensitivity metric to rank order joints based on their influence towards the dynamics of the assembled structure. Results are compared against local gradient-based and global sampling-based metrics as part of two numerical examples.

1. Introduction

Complex engineering structures (such as vehicles, satellites, domestic products, buildings and more) are built-up from individual components that are joined with connections that rely on frictional contact or other dissipative mechanisms (such as elastomeric elements). To model such a structure it is conventional to follow a component-based strategy, where individual components are measured, or modelled, independently of one another, before being assembled to form the complete model. Typically, this assemblage is achieved by enforcing equilibrium and continuity conditions (or energetic equivalents) at the connecting interfaces between components; a process referred to as sub-structuring [1]. This is, however, an idealisation. The joints that connect components possess their own dynamics; ideal rigid coupling is rarely achieved in practice. Importantly, these joint dynamics can have a significant impact on the performance, or even survivability, of an operational assembly [2]. Hence, when adopting a component-based strategy, it is essential that, where necessary, jointed connections are characterised and modelled appropriately.

The types of joints encountered in practical engineering structures are wide ranging, and can include bolted connections, rivets, welds, and resilient elements, among many others [3]. Likewise, their dynamics can vary greatly, from linear spring or beam-like coupling, to non-linear hysteretic, perhaps discontinuous (e.g. frictional), connections [4,5]. Whether linear or non-linear, two principal issues arise when modelling complex jointed structures.

First, an experimental characterisation of each joint is required before they can be represented within a component-based model. This characterisation is an experimentally demanding task [6–11], often reinquiring supplementary numerical models [12–14]. As an example, in [6,7,9] the experimental procedure involves measuring the point and transfer admittance between the interface/joint and a set of remote DoFs on both the assembled and individual components. In [12] the individual component admittances are instead obtained by FE models. In [13,14] the need for interface-based measurements is avoided using a hybrid

E-mail address: j.w.r.meggitt1@salford.ac.uk.

https://doi.org/10.1016/j.jsv.2022.116850
Received 7 June 2021; Received in revised form 10 February 2022; Accepted 14 February 2022
Available online 5 March 2022

experimental/numerical 'System Equivalent Model Mixing' scheme, though several remote measurements are still required on the connected components. For a non-linear characterisation experimental efforts are multiplied, often requiring controlled shaker excitations with increasing amplitude levels [11] or advanced time domain identification methods [10]. As an alternative to experimental characterisation, joint characteristics might be obtained indirectly by model updating [15,16].

Second, the computational effort required to incorporate a non-linear or 3D elastic joint model can be many times greater than that of a linear or 1D joint [17,18]. For complex built-up structures, where many joints are present, these efforts are multiplied, and a complete characterisation/modelling of all joints is often not feasible. Hence, in the development or refinement of a component-based model there is a need to identify the *response-critical joints* of an assembly – those that have the greatest influence on the target response – so that experimental and computational resources may be focused towards those joints which will benefit the modelling effort most. Importantly, the influence of a specific joint will depend not only on the passive dynamics of its connected components, but also on the operational activity of the assembly.

It is worth noting that the identification of 'critical joints' is often considered in the context of structural analysis, where joints that experience high static loads are identified and subject to local non-linear reanalysis [16]. In the present paper we consider, instead, the *dynamic* response of an assembled structure, and the relative importance of individual joints towards said response. We address the issue of response-critical joint identification by considering an interval-based sensitivity analysis (SA) of the assembled structure's response, with respect to the relaxation of individual interface connections.

When dealing with problems of uncertainty, such as sensitivity analysis (SA), are two common view points: probabilistic or non-probabilistic. SA is typically treated probabilistically, describing uncertain parameters by their probability distributions. A principal difficulty here is that to evaluate the uncertainty of a complex system by probabilistic means, detailed statistical input data is required. If this data is not available, complex statistical analysis cannot be justified. This issue can be overcome by non-probabilistic, or 'possibilistic', analysis methods, which include: interval analysis [19–25], convex modelling [26] and fuzzy set theory [27,28]. Possibilistic methods do not consider the probability of an outcome occurring, rather whether or not is it *possible*.

Joint characterisation is an experimentally demanding task, and so it is often challenging to obtain the statistical information required to conduct a conventional probabilistic analysis of uncertainty. Possibilistic, or interval analysis, methods offer a convenient alternative. Interval-based methods have found numerous applications in the analysis of structural dynamic systems, including; interval Finite Element Analysis [20,21], eigenfrequency analysis [29,30], robustness evaluation [31], quantification of experimental uncertainty [25], inverse force identification [23], stochastic response analysis [32,33], among many others. In the present paper, we consider its application towards the identification of response-critical joints.

Based on the rank ordering of a proposed sensitivity metric, we are able to infer the relative importance of individual joints by their contribution towards the global dynamics of the assembled structure. The proposed metric is formulated by considering the dual formulation of the sub-structuring problem in the presence of a flexible interface [34]. The Sherman–Morrison formula is used to separate out the contribution of an individual joint, at which point a complex interval description is adopted for the interface stiffness and damping. Employing interval arithmetic, the maximum and minimum bounds of the coupled assembly admittance (also operational response) are determined. Spatial averaging of the interval bounds over selected degrees of freedom (DoFs) yields a metric that indicates the relative importance of a particular joint towards the dynamics of the assembled structure, in a possibilistic sense. Results are compared against local gradient-based and global sampling-based (Sobol) metrics, also proposed herein.

Having introduced its context and principal aim, the remainder of this paper will be structured as follows. Section 2 will begin by introducing the notion of real and complex intervals, alongside their arithmetic operations. Primal and dual approaches to modelling flexible interface dynamics are then summarised in Section 3, before Section 4 details the proposed interval-based assessment of joint variability. Section 5 then considers the identification of response-critical joints, before Section 6 presents two numerical examples and Section 7 draws some concluding remarks.

2. Interval arithmetic

Interval analysis falls within a family of non-probabilistic methods for evaluating uncertainty in complex systems [35,36]. One of the principal difficulties in evaluating the uncertainty of a complex system by probabilistic means is the acquirement of detailed statistical input data. In the absence of such data, complex statistical analysis cannot be justified. It is this issue that has lead to the development of non-probabilistic, or 'possibilistic', methods, to which interval analysis belongs.

2.1. Real intervals

A real interval $\{x\} = [\underline{x} \quad \overline{x}]$ (denoted by curly braces) is represented by two numbers forming the upper ($\overline{x}$) and lower ($\underline{x}$) bounds of the unknown variable x,

$$\underline{x} < x < \overline{x}. \tag{1}$$

Unlike a probability distribution, the interval bounds provide no detailed information on the likeliness of a particular value of x, only that its true value must occur within it.

With the definition of an interval, as per Eq. (1), it is the role of interval arithmetic to compute the upper and low bounds of functions whose inputs are intervals. This is achieved by redefining the basic arithmetic operations $+ \; - \; \times \; \div$ as interval operations $\oplus \; \ominus \; \otimes \; \oslash$.

For real valued x and y, the key interval arithmetic operations are defined as [37]:

$$\{x\} \oplus \{y\} = [\underline{x} \quad \overline{x}] \oplus [\underline{y} \quad \overline{y}] = [\underline{x} + \underline{y} \quad \overline{x} + \overline{y}] \tag{2}$$

$$\{x\} \ominus \{y\} = [\underline{x} \quad \overline{x}] \ominus [\underline{y} \quad \overline{y}] = [\underline{x} - \overline{y} \quad \overline{x} - \underline{y}] \tag{3}$$

$$\{x\} \otimes \{y\} = [\underline{x} \quad \overline{x}] \otimes [\underline{y} \quad \overline{y}] = [\min(\underline{x}\underline{y}, \underline{x}\overline{y}, \overline{x}\underline{y}, \overline{x}\overline{y}) \quad \max(\underline{x}\underline{y}, \underline{x}\overline{y}, \overline{x}\underline{y}, \overline{x}\overline{y})] \tag{4}$$

$$\{x\} \oslash \{y\} = [\underline{x} \quad \overline{x}] \otimes [1/\overline{y} \quad 1/\underline{y}] \qquad \text{if} \quad 0 \notin [\underline{y} \quad \overline{y}] \tag{5}$$

Care should be taken with interval division; if the interval $\{y\}$ contains zero, its reciprocal will extend to $\pm\infty$.

Note that non-interval quantities can readily be incorporated within the interval arithmetic presented above by considering an interval whose upper and lower bounds are of equal value, $x = \{x\} = [x \quad x]$. More complex interval functions can be dealt with by recursively applying these arithmetic operations.

2.2. Complex intervals

There are two common ways in which interval arithmetic can be extended to complex variables. In one, the complex interval is represented by a circular disk in the complex plane, characterised by its centre point and radius [37,38]. In the other, the real and imaginary parts of the complex number are represented by independent real intervals. This leads to a rectangular interval in the complex plane [37,39,40]. The rectangular approach has the advantage that the real and imaginary parts can be assigned different intervals, which is not possible via the circular disk representation, which assumes an inherent interdependency. In the present paper we will adopt the rectangular complex interval approach as it will enable the independent assignment of joint stiffness and damping.

Taking x and y now to be complex numbers, their rectangular intervals take the form,

$$\{x\} = \{x_r\} + i\{x_i\}, \qquad \{y\} = \{y_r\} + i\{y_i\} \tag{6}$$

where,

$$\{x_r\} = [\underline{x}_r \quad \overline{x}_r], \quad \{x_i\} = [\underline{x}_i \quad \overline{x}_i], \quad \{y_r\} = [\underline{y}_r \quad \overline{y}_r], \quad \{y_i\} = [\underline{y}_i \quad \overline{y}_i]. \tag{7}$$

These intervals describe rectangular domains in the complex plane, as illustrated in Fig. 1 (orange and yellow rectangles). To analyse complex interval functions we must extend the interval arithmetic defined above to the complex domain. For non-interval complex variables, addition, subtraction and multiplication can be defined as,

$$x + y = (x_r + y_r) + i(x_i + y_i), \quad x - y = (x_r - y_r) + i(x_i - y_i), \quad x \times y = (x_r y_r - x_i y_i) + i(x_r y_i + x_i y_r). \tag{8}$$

Based on the above, an equivalent set of complex interval operations can be defined as,

$$\{x\} \oplus \{y\} = \{x_r\} \oplus \{y_r\} + i\{x_i\} \oplus \{y_i\} = [\underline{x}_r + \underline{y}_r \quad \overline{x}_r + \overline{y}_r] + i[\underline{x}_i + \underline{y}_i \quad \overline{x}_i + \overline{y}_i] \tag{9}$$

$$\{x\} \ominus \{y\} = \{x_r\} \ominus \{y_r\} + i\{x_i\} \ominus \{y_i\} = [\underline{x}_r - \overline{y}_r \quad \overline{x}_r - \underline{y}_r] + i[\underline{x}_i - \overline{y}_i \quad \overline{x}_i - \underline{y}_i] \tag{10}$$

$$\{x\} \otimes \{y\} = \left(\{x_r\} \otimes \{y_r\} \ominus \{x_i\} \otimes \{y_i\}\right) + i\left(\{x_r\} \otimes \{y_i\} \oplus \{x_i\} \otimes \{y_r\}\right) \tag{11}$$

where $\oplus$, $\ominus$ and $\otimes$ are defined as per the real interval operations.

These complex interval operations are optimal; they provide the smallest rectangular interval that includes the set of all possible outcomes. Shown in Fig. 1abc are the complex intervals arising due to $\{x\} \oplus \{y\}$, $\{x\} \ominus \{y\}$ and $\{x\} \otimes \{y\}$, respectively, where $\{x\}$ and $\{y\}$ are the complex intervals represented by the yellow and orange rectangles. Results are compared against a sampling-based estimation (blue dots). Note that in using the rectangular interval description described above, addition and subtraction do not alter the shape of the interval. Multiplication, on the other hand, leads to a change in shape. Hence, the interval description over estimates the true region of possible outcomes. Nevertheless, the resulting interval is still optimum in a rectangular sense.

Let us now consider the case of complex division, defined as,

$$x \div y = \frac{x_r y_r + x_i y_i}{y_r^2 + y_i^2} + i\,\frac{x_i y_r - x_r y_i}{y_r^2 + y_i^2}. \tag{12}$$

Applying the above interval operations yields the following,

$$\{x\} \oslash \{y\} = \left(\{x_r\} \otimes \{y_r\} \oplus \{x_i\} \otimes \{y_i\}\right) \oslash \left(\{y_r^2\} \oplus \{y_i^2\}\right) + i\left(\{x_i\} \otimes \{y_r\} \ominus \{x_r\} \otimes \{y_i\}\right) \oslash \left(\{y_r^2\} \oplus \{y_i^2\}\right). \tag{13}$$

The complex interval obtained as per Eq. (13) is *not* optimal. If standard interval arithmetic operations are applied to complex division, the numerator and denominator intervals are treated *independently* (the so-called dependency problem). For example, the instance of $\{y_r\}$ in the numerator is considered independent to that being squared in the denominator $\{y_r^2\}$. The same issues occurs with $\{y_i\}$. This can lead to a huge over estimation of the interval, as illustrated by the grey rectangle in Fig. 1d. Similar

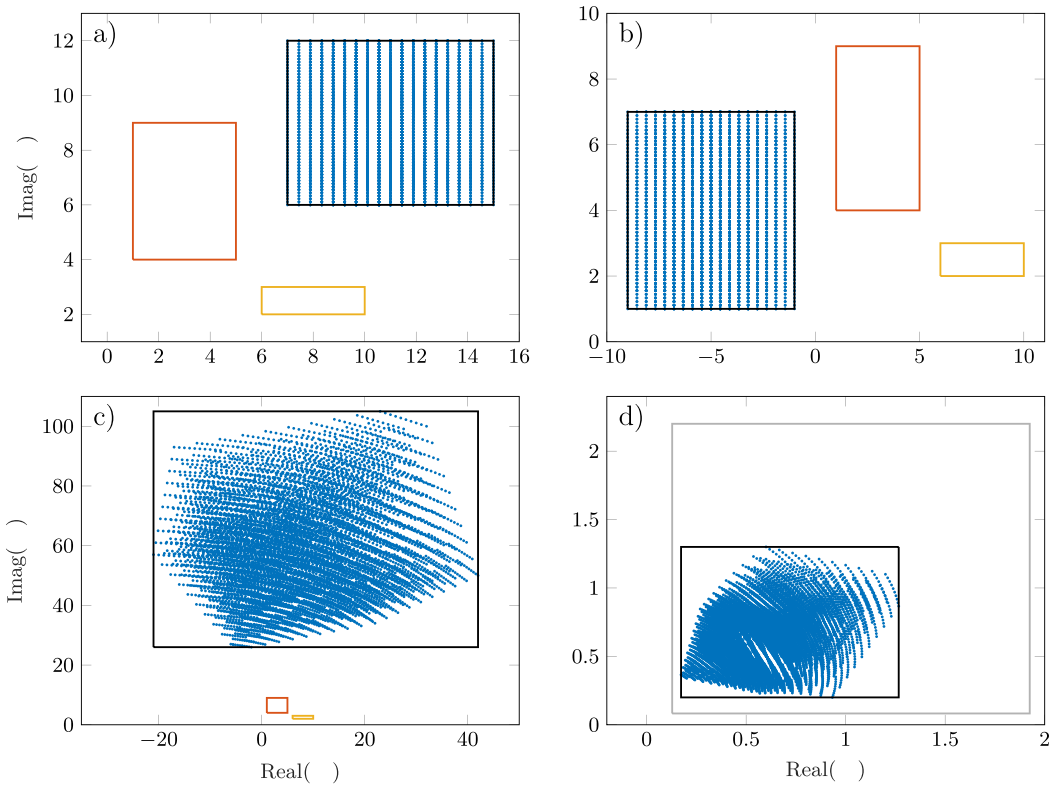

Fig. 1. Interval operations applied to the complex intervals $\{x\} = \{x_r\} + i\{x_i\}$ and $\{y\} = \{y_r\} + i\{y_i\}$ shown in yellow and orange, respectively: (a) addition $\{x\} \oplus \{y\}$, (b) subtraction $\{x\} \ominus \{y\}$, (c) multiplication $\{x\} \otimes \{y\}$, and (d) division $\{x\} \oslash \{y\}$ (grey box — naive implementation, black box — optimum rectangular bound [41]). Note that the intervals $\{x\}$ and $\{y\}$ are omitted from (d) to more clearly show the over estimation caused by the dependency problem. (For interpretation of the references to colour in this figure legend, the reader is referred to the web version of this article.)

dependency issues are often encountered for more complex functions of interval input parameters and represent one of the main limiting factors of conventional interval analysis. For complex division, special algorithms are required to compute the optimal rectangular interval [39–41]. See for example the black interval in Fig. 1d, which was obtained as per the algorithm presented in [41].

In the present work these algorithms are not well suited as the intervals used to describe a joint's dynamics will extend from some minimum stiffness/damping value, to infinity (representing a rigid joint). Hence, we propose an alternative algorithm to determine the rectangular bounds for the special case of complex division considered here (see Appendix A).

3. Flexible interface dynamics in complex built-up structures

For the sake of clarity, we consider two arbitrary components A and B coupled via N spring–damper joints J that connect the interface DoFs c (see Fig. 2). Though, the developments below are easily generalised to more complex assemblies. Our intention is to consider the dynamics of this structure when a joint's characteristics are described in terms of a complex interval, whose upper bounds extend to infinity (i.e. representing a rigid coupling). To this end, we first present the primal and dual sub-structuring formulations in the presence of flexible interface dynamics. The reader is referred to the many well established texts for further details on the primal and dual sub-structuring formulations [1,42].

For linear time invariant structures it is well known that the dynamics of a structural component can be described by the equation of motion (EoM),

$$\mathbf{M}_i\ddot{\mathbf{u}}(t) + \mathbf{R}_i\dot{\mathbf{u}}(t) + \mathbf{K}_i\mathbf{u}(t) = \mathbf{f}(t) + \mathbf{g}(t) \tag{14}$$

where $\mathbf{M}_i$, $\mathbf{R}_i$ and $\mathbf{K}_i$ represent the discretised mass, damping and stiffness matrices of the ith component, $\mathbf{u}$ is a vector of displacements with $\dot{\square}$ denoting differentiation wrt. time, $\mathbf{f}$ is a vector of externally applied forces, and $\mathbf{g}$ a vector of internal coupling forces [43].

Assuming time harmonic motion, Eq. (14) may be transformed into a more convenient frequency domain representation,

$$\left(-\omega^2\mathbf{M}_i + i\omega\mathbf{R}_i + \mathbf{K}_i\right)\mathbf{u}(\omega) = \mathbf{f}(\omega) + \mathbf{g}(\omega) \tag{15}$$

from which we can define the dynamic stiffness matrix,

$$\mathbf{Z}_i = -\omega^2\mathbf{M}_i + i\omega\mathbf{R}_i + \mathbf{K}_i. \tag{16}$$

Alternatively, the dynamic stiffness matrix can be obtained through the inversion of a measured or modelled admittance matrix,

$$\mathbf{Z}_i = \mathbf{Y}_i^{-1}. \tag{17}$$

The component EoM then becomes,

$$\mathbf{Z}_i\mathbf{u}(\omega) = \mathbf{f}(\omega) + \mathbf{g}(\omega). \tag{18}$$

The purpose of (frequency-based) sub-structuring is to obtain the equation of motion, dynamic stiffness, or admittance matrix of a multi-component structure based on those of its individual components. There exist two common formulations for doing so, primal and dual.

3.1. Primal

The EoM representing the *uncoupled* AJB system are obtained by block-diagonalising the component EoMs (explicit frequency dependence has been omitted for clarity),

$$\mathbf{Z}\mathbf{u} = \mathbf{f} + \mathbf{g} \tag{19}$$

where $\mathbf{Z}$ is a block diagonal dynamic stiffness matrix, $\mathbf{u}$, $\mathbf{f}$, and $\mathbf{g}$ are stacked response, external force and interface force vectors, respectively. Importantly, the primal formulation considers the joint as an *independent component* such that,

$$\mathbf{Z} = \begin{bmatrix} \mathbf{Y}_A^{-1} & & \\ & \mathbf{Z}_J & \\ & & \mathbf{Y}_B^{-1} \end{bmatrix} \tag{20}$$

where $\mathbf{Y}_A^{-1}$ and $\mathbf{Y}_B^{-1}$ are the inverse admittance matrices of components A and B, and $\mathbf{Z}_J$ is the joint dynamic stiffness matrix. For the spring–damper joint considered,

$$\mathbf{Z}_J = \begin{bmatrix} \begin{pmatrix} k+ir & -k-ir \\ -k-ir & k+ir \end{pmatrix}_1 & & \\ & \ddots & \\ & & \begin{pmatrix} k+ir & -k-ir \\ -k-ir & k+ir \end{pmatrix}_N \end{bmatrix} \tag{21}$$

where k is the joint stiffness, and r its damping coefficient. To assemble the AJB system the conditions of continuity and equilibrium must be satisfied. These are expressed concisely in matrix form, respectively, by,

$$\mathbf{B}\mathbf{u} = \mathbf{0}, \tag{22}$$

and

$$\mathbf{L}^{\mathrm{T}}\mathbf{g} = \mathbf{0} \tag{23}$$

where $\mathbf{B}$ and $\mathbf{L}$ represent signed and unsigned Boolean matrices [1]. The primal formulation continues by defining a new response vector $\mathbf{u}_C$ that belongs to the assembled structure. Continuity is then satisfied by relating the two response vectors (coupled and uncoupled) as so,

$$\mathbf{u} = \mathbf{L}\mathbf{u}_C. \tag{24}$$

By substituting Eq. (24) into Eq. (19), and pre-multiplying all terms by $\mathbf{L}^{\mathrm{T}}$ (hence satisfying Eq. (23)) we obtain,

$$\mathbf{L}^{\mathrm{T}}\mathbf{Z}\mathbf{L}\mathbf{u}_C = \mathbf{L}^{\mathrm{T}}\mathbf{f} \tag{25}$$

or equivalently,

$$\mathbf{u}_C = \mathbf{Y}_C\mathbf{f}_C \tag{26}$$

where $\mathbf{f}_C = \mathbf{L}^{\mathrm{T}}\mathbf{f}$ is the external force applied to the coupled assembly, and

$$\mathbf{Y}_C = \left(\mathbf{L}^{\mathrm{T}}\begin{bmatrix} \mathbf{Y}_A^{-1} & & \\ & \mathbf{Z}_J & \\ & & \mathbf{Y}_B^{-1} \end{bmatrix}\mathbf{L}\right)^{-1} \tag{27}$$

is the coupled admittance of the $C = AJB$ assembly.

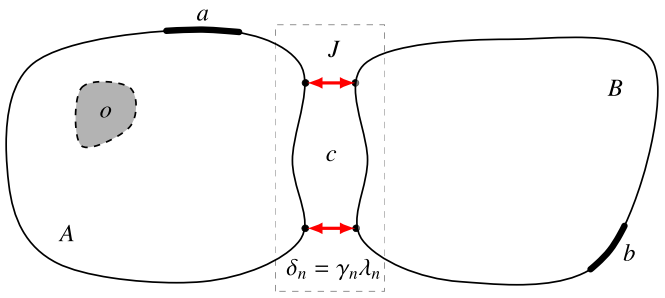

Fig. 2. General active–passive assembly (AJB) with interface flexibility. The relative interface displacement at the nth connection $\delta_n = u_{An} - u_{Bn}$ is proportional to the interface flexibility γ_n and the internal coupling force λ_n. a and b represent remote source and receiver DoFs, c are the interface DoFs, and o is the internal region where operational forces develop if A were an active component.

Importantly, according to the primal procedure, a joint is represented by its dynamic stiffness matrix. Whilst in this form we are able to accept arbitrarily complex joints, including inertial effects, an ideal rigid coupling would require the joint stiffness to tend to infinity. This complicates the investigation of joint relaxation. Fortunately, a more convenient (albeit less general) form can be derived following the dual sub-structuring formulation.

3.2. Dual

Unlike the primal formulation, which considers the joint as a separate component, the dual formulation treats the joint as a relaxation of the continuity condition. In the presence of a flexible interface, for example due to the spring–damper joint, continuity is not satisfied. Instead,

$$\mathbf{B}\mathbf{u} = \delta = \boldsymbol{\Gamma}\lambda \tag{28}$$

where the interface separation δ is related to the unknown joint force λ by an interface flexibility matrix $\boldsymbol{\Gamma}$. For the spring–damper joint considered, this flexibility matrix is given by,

$$\boldsymbol{\Gamma} = \begin{bmatrix} \left(\frac{1}{k+ir}\right)_1 & & \\ & \ddots & \\ & & \left(\frac{1}{k+ir}\right)_N \end{bmatrix} = \begin{bmatrix} (\gamma_r + i\gamma_i)_1 & & \\ & \ddots & \\ & & (\gamma_r + i\gamma_i)_N \end{bmatrix} \tag{29}$$

where,

$$\gamma_r = \frac{k}{|Z|^2}, \quad \gamma_i = -\frac{r}{|Z|^2}, \quad \text{and} \quad Z = k + ir. \tag{30}$$

To satisfy equilibrium, the interface force $\mathbf{g}$ is given the form,

$$\mathbf{g} = -\mathbf{B}^{\mathrm{T}}\lambda \tag{31}$$

where λ are the unknown joint forces and $\mathbf{B}$ is a signed Boolean matrix. The presence of $\mathbf{B}^{\mathrm{T}}$ ensures that the forces applied to components A and B are equal and opposite, thus satisfying equilibrium.

The unknown joint forces λ are found using the relaxed continuity condition as follows. The interface force $\mathbf{g}$ is substituted into Eq. (19), to give,

$$\mathbf{u} = \mathbf{Y}\left(\mathbf{f} - \mathbf{B}^{\mathrm{T}}\lambda\right). \tag{32}$$

where $\mathbf{Y} = \mathbf{Z}^{-1}$ has been used. Note that $\mathbf{Y}$, as per the dual approach, does not contain a joint admittance matrix ($\mathbf{Z}_J$ is non-invertible); instead the joint is accounted for by Eq. (28). Eq. (32) is substituted into the relaxed continuity condition (Eq. (28)),

$$\mathbf{B}\mathbf{Y}\left(\mathbf{f} - \mathbf{B}^{\mathrm{T}}\lambda\right) = \boldsymbol{\Gamma}\lambda. \tag{33}$$

Solving for λ then yields,

$$\lambda = \left(\mathbf{B}\mathbf{Y}\mathbf{B}^{\mathrm{T}} + \boldsymbol{\Gamma}\right)^{-1}\mathbf{B}\mathbf{Y}\mathbf{f}. \tag{34}$$

Finally, substituting Eq. (34) into Eq. (32) leads to,

$$\mathbf{u} = \mathbf{Y}_C\mathbf{f} \tag{35}$$

where,

$$\mathbf{Y}_C = \mathbf{Y} - \mathbf{Y}\mathbf{B}^{\mathrm{T}}\left(\mathbf{B}\mathbf{Y}\mathbf{B}^{\mathrm{T}} + \boldsymbol{\Gamma}\right)^{-1}\mathbf{B}\mathbf{Y} \tag{36}$$

is the coupled admittance of the $C = AJB$ assembly. The advantage of this form of $\mathbf{Y}_C$ is that a rigidly connected system is obtained by taking the limit as $\boldsymbol{\Gamma} \to \mathbf{0}$ (i.e. $k, r \to \infty$), as opposed to $\mathbf{Z}_J \to \infty$. This simplifies the derivation of an interface sensitivity metric which can be used to identify response-critical joints.

4. Interval-based assessment of joint dynamics

In this section we will consider an interval-based representation of joint dynamics, and its application in determining the maximum and minimum bounds of an assembled structure's admittance matrix due to an interface relaxation. As shown in Section 3.2, the dual formulation, in the presence of a flexible interface, leads to the following equation for the assembled admittance matrix,

$$\mathbf{Y}_C = \mathbf{Y} - \mathbf{Y}\mathbf{B}^{\mathrm{T}} \left(\mathbf{B}\mathbf{Y}\mathbf{B}^{\mathrm{T}} + \boldsymbol{\Gamma}\right)^{-1} \mathbf{B}\mathbf{Y} \tag{37}$$

where the interface flexibility matrix $\boldsymbol{\Gamma}$ is defined as,

$$\boldsymbol{\Gamma} = \begin{bmatrix} \gamma_1 & & & \\ & \gamma_2 & & \\ & & \ddots & \\ & & & \gamma_N \end{bmatrix}, \qquad \gamma = \frac{1}{k + ir} = \gamma_r + i\gamma_i, \qquad \gamma_r = \frac{k}{|Z|^2}, \qquad \gamma_i = -\frac{r}{|Z|^2}, \quad \text{and} \quad Z = k + ir. \tag{38}$$

With attention focused towards the influence of a single joint, it is convenient to separate its contribution by means of the Sherman–Morrison formula (rank-one update) [44],

$$(\mathbf{A} + \mathbf{X})^{-1} = \mathbf{A}^{-1} - \frac{1}{1 + \mathrm{tr}\left(\mathbf{X}\mathbf{A}^{-1}\right)} \mathbf{A}^{-1}\mathbf{X}\mathbf{A}^{-1}, \tag{39}$$

where $\mathbf{A}$ is any invertible matrix, and $\mathbf{X}$ is a matrix of rank 1. To apply the Sherman–Morrison formula, the interface flexibility matrix $\boldsymbol{\Gamma}$ is split into two parts; $\boldsymbol{\Gamma}^{(n)}$, which contains the nth joint flexibility of interest, and $\boldsymbol{\Gamma}^{(\sim n)}$, which contains all remaining terms,

$$\boldsymbol{\Gamma}^{(\sim n)} = \begin{bmatrix} \gamma_1 & & & \\ & \gamma_2 & & \\ & & \ddots & \\ & & & 0 \end{bmatrix}, \qquad \boldsymbol{\Gamma}^{(n)} = \begin{bmatrix} 0 & & & \\ & 0 & & \\ & & \ddots & \\ & & & \gamma_n \end{bmatrix}, \qquad \boldsymbol{\Gamma} = \boldsymbol{\Gamma}^{(\sim n)} + \boldsymbol{\Gamma}^{(n)}. \tag{40}$$

Note that $\boldsymbol{\Gamma}^{(n)}$ is a rank one matrix, so can take on the role of $\mathbf{X}$ in Eq. (39). Hence, the matrix inverse in Eq. (37) can be rewritten in the form,

$$\left(\mathbf{B}\mathbf{Y}\mathbf{B}^{T} + \boldsymbol{\Gamma}^{(\sim n)} + \boldsymbol{\Gamma}^{(n)}\right)^{-1} = \left(\mathbf{A} + \boldsymbol{\Gamma}^{(n)}\right)^{-1} = \mathbf{A}^{-1} - \frac{1}{1 + \mathrm{tr}\left(\boldsymbol{\Gamma}^{(n)}\mathbf{A}^{-1}\right)} \mathbf{A}^{-1}\boldsymbol{\Gamma}^{(n)}\mathbf{A}^{-1} \tag{41}$$

where $\mathbf{A} = \mathbf{B}\mathbf{Y}\mathbf{B}^{T} + \boldsymbol{\Gamma}^{(\sim n)}$. Note that $\boldsymbol{\Gamma}^{(n)}$ is a single entry matrix. Its only non-zero value, the interface flexibility γ_n, can be brought out as a scalar term, and $\boldsymbol{\Gamma}^{(n)}$ replaced by $\mathbf{P}_n$, which is a zero matrix bar the nth diagonal entry whose value is 1. Eq. (41) then reduces to,

$$\left(\mathbf{B}\mathbf{Y}\mathbf{B}^{T} + \boldsymbol{\Gamma}^{(\sim n)} + \boldsymbol{\Gamma}^{(n)}\right)^{-1} = \mathbf{A}^{-1} - w_n \mathbf{A}^{-1}\mathbf{P}_n\mathbf{A}^{-1} \tag{42}$$

where,

$$w_n = \frac{\gamma_n}{1 + \mathrm{tr}\left(\mathbf{P}_n\mathbf{A}^{-1}\right)\gamma_n} = \frac{1}{\frac{1}{\gamma_n} + \mathrm{tr}\left(\mathbf{P}_n\mathbf{A}^{-1}\right)} = \frac{1}{Z_n + \mathrm{tr}\left(\mathbf{P}_n\mathbf{A}^{-1}\right)} \tag{43}$$

is a complex scalar value, and $Z_n = k_n + ir_n$ is the dynamic stiffness of the nth interface connection. Note that w_n is a non-linear function of γ_n; the joint flexibility, although linear in its dynamics, has a non-linear effect on the assembled structure.

Herein we propose that the interface stiffness Z_n be treated as a complex interval $\{Z_n\}$, such that its bounds are supposed to contain all possible values of joint stiffness and damping, including those of a rigid connection. The complex interval $\{Z\} = \{k\} + i\{r\}$ is characterised by a pair of real intervals, namely $\{k\} = [\underline{k} \quad \overline{k}]$ and $\{r\} = [\underline{r} \quad \overline{r}]$, where $\underline{\square}$ and $\overline{\square}$ denote, respectively, lower and upper bounds. In particular, we are interested in the case that $\overline{k} = \overline{r} = \infty$, i.e. a rigid connection. That is, we are interested in the range of possible outcomes given the relaxation of a rigid connection.

Treating the interface stiffness as a complex interval $\{Z_n\}$, Eq. (43) now describes a complex interval reciprocal,

$$\{w_n\} = 1 \oslash \left[\{Z_n\} \oplus \mathrm{tr}\left(\mathbf{P}_n\mathbf{A}^{-1}\right)\right] = 1 \oslash \{z_n\} \tag{44}$$

where $\{z_n\} = \{Z_n\} \oplus \mathrm{tr}\left(\mathbf{P}_n\mathbf{A}^{-1}\right) = \{x\} + i\{y\}$. In Appendix A we present a straightforward approach to determine the bounds of the complex interval $\{w_n\}$, given $\{x\} = [\underline{x} \quad \infty]$ and $\{y\} = [\underline{y} \quad \infty]$.

Having determined the interval bounds of $\{w_n\}$, substituting Eq. (42) and (44) into Eq. (37), leads to the interval expression,

$$\{\mathbf{Y}_C\} = \underbrace{\mathbf{Y} - \mathbf{Y}\mathbf{B}^{T}\left(\mathbf{B}\mathbf{Y}\mathbf{B}^{T} + \boldsymbol{\Gamma}^{(\sim n)}\right)^{-1}\mathbf{B}\mathbf{Y}}_{\text{Coupled with rigid } n} \oplus \left[\underbrace{\{w_n\} \otimes \mathbf{Y}\mathbf{B}^{T}\left(\mathbf{B}\mathbf{Y}\mathbf{B}^{T} + \boldsymbol{\Gamma}^{(\sim n)}\right)^{-1}\mathbf{P}_n\left(\mathbf{B}\mathbf{Y}\mathbf{B}^{T} + \boldsymbol{\Gamma}^{(\sim n)}\right)^{-1}\mathbf{B}\mathbf{Y}}_{\text{Interval matrix describing joint relaxation}}\right] \tag{45}$$

or

$$\{\mathbf{Y}_C\} = \mathbf{Y}_C^{(\sim n)} \oplus \left\{ \Delta\mathbf{Y}_C^{(n)} \right\} = \mathbf{Y}_C^{(\sim n)} \oplus \left[\mathbf{J}_n \otimes \{w_n\} \right] \tag{46}$$

where $\mathbf{J}_n$ is the Jacobian matrix that contains the partial derivatives of the coupled assembly admittance with respect to the nth interface flexibility (see Section Section 5.1) , and $\{\mathbf{Y}_C\}$ is a complex interval admittance matrix whose bounds enclose all possible values obtainable given the range of permissible joint dynamics specified by the interval $\{Z_n\}$.

Note that $\mathbf{Y}_C^{(\sim n)}$ contains no intervals, and represent the structure's admittance when $\gamma_n = 0$, i.e. when the nth contact is made rigid. Hence, $\left\{ \Delta\mathbf{Y}_C^{(n)} \right\}$ represents an interval matrix that describes the effect, or influence, of the nth joint's relaxation on the coupled admittance.

4.1. Response interval

In the presence of an active component (i.e. a vibration source) the operational response $\mathbf{u}_C$ is often of greater importance than the assembly admittance. Hence, we look to extend the interval treatment above to account for an assembly's operational activity.

The operational response of a complex assembly can be expressed in the form,

$$\mathbf{u}_C = \mathbf{Y}_C \bar{\mathbf{f}}_S \tag{47}$$

where $\mathbf{Y}_C$ is the coupled admittance matrix, and $\bar{\mathbf{f}}_S$ is a vector of so called *blocked forces* [45]. The blocked force is an independent source quantity that describes its operational activity. It has become an internationally standardised method for experimentally characterising vibratory sources [46], and is used extensively across several engineering sectors, including: automotive [47,48], railway [49,50], heavy machinery [51] and building acoustics [52].

As per Eq. (47), the complex interval of an operational response can be obtained by,

$$\left\{\mathbf{u}_C\right\} = \left\{\mathbf{Y}_C\right\} \otimes \bar{\mathbf{f}}_S = \mathbf{u}_C^{(\sim n)} \oplus \left[\left\{ \Delta\mathbf{Y}_C^{(n)} \right\} \otimes \bar{\mathbf{f}}_S \right] = \mathbf{u}_C^{(\sim n)} \oplus \left\{ \Delta\mathbf{u}_C^{(n)} \right\}. \tag{48}$$

where it is noted that $\otimes$ represents an interval matrix multiplication. Like the assembly admittance, the interval response is made up of two parts; the first is that of the assembly when the nth joint is considered rigid $\mathbf{u}_C^{(\sim n)}$, and the second is an interval contribution describing a relaxation of the nth joint $\left\{ \Delta\mathbf{u}_C^{(n)} \right\}$.

5. Identification of response-critical joints

The principal aim of this paper is to provide an efficient identification of the response-critical joints within a complex built-up structure. Here, response-critical joints are deemed as those whose refinement would benefit the modelling effort most. In what follows we propose three sensitivity metrics for this purpose; a local gradient-based, a global sampling-based, and a pseudo-global interval-based metric.

Sensitivity analysis (SA) is a tool used to allocate, or apportion, the uncertainty in a system's output to that of its input parameters [53]. Methods of SA can be broadly categorised as local or global. Local methods assume a small variance on the input parameters and consider a linearisation of the system's dynamics. Such methods are typically based on partial derivatives (obtained analytically or by numerical approximation), much like a typical error propagation [54]. Local methods are advantageous in terms of computational efficiency, but limited in terms of accuracy, especially for non-linear systems with reasonable levels of input variance. Global methods overcome this limitation by sampling the model output over the space of input parameters. Whilst computationally more expensive, this approach ensures that model non-linearity and input parameter distributions are accounted for. Hence, more a robust analysis is achieved.

In the context of response-critical joints, a naive identification might consider the Jacobian matrix (containing the partial derivatives of the coupled admittance with respect to each joint parameter) alone, which describes the local sensitivity of the coupled assembly based on a infinitesimal relaxation of the interface. Clearly, this does not account for the non-linear contribution of a joint's dynamics to those of the coupled structure (see Eq. (43)). An alternative approach might be to consider a global sampling-based strategy, using metrics such as the Sobol indices [55], to identify and rank order response-critical joints. Whilst a robust approach, providing sufficient samples are drawn, for a system with many joints the computational effort may become prohibitive. Furthermore, in the absence of detailed statistical information, it is unclear how a joint's dynamics should be represented. Herein, we propose an interval-based sensitivity metric to identify the response-critical joints of an assembly. Its computational effort is not too dissimilar to that of the Jacobian-based approach, whilst its application extends beyond the assumption of an infinitesimal relaxation; it can be applied in the presence of an arbitrary relaxation. Whilst the interval approach considers the entire input space (defined by the joint interval $\{Z\}_n$), it does not provide the detailed information offered by a global sampling-based approach, hence we term this approach a pseudo-global method.

In what follows we introduce three sensitivity metrics, based on the above strategies (local, global and pseudo-global), to rank order the influence of individual joints towards the dynamics of the global assembly.

5.1. Gradient-based sensitivity

To develop a gradient-based sensitivity metric we first derive the system's Jacobian matrix, representing the derivative of the assembly admittance with respect to a specific joint's flexibility. We begin by considering the complex differential of the assembly admittance,

$$\mathrm{d}\mathbf{Y}_C = \mathrm{d}\left(\mathbf{Y}\right) - \mathrm{d}\left(\mathbf{Y}\mathbf{B}^T\left(\mathbf{B}\mathbf{Y}\mathbf{B}^T + \boldsymbol{\Gamma}\right)^{-1}\mathbf{B}\mathbf{Y}\right). \tag{49}$$

Noting that interest lies in the differential interface flexibility $\mathrm{d}(\boldsymbol{\Gamma})$, the above reduces to,

$$\mathrm{d}\mathbf{Y}_C = -\mathrm{d}\left(\mathbf{Y}\mathbf{B}^T\left(\mathbf{B}\mathbf{Y}\mathbf{B}^T + \boldsymbol{\Gamma}\right)^{-1}\mathbf{B}\mathbf{Y}\right). \tag{50}$$

Application of the product rule, $\mathrm{d}\left(\mathbf{ABC}\right) = \mathrm{d}\left(\mathbf{A}\right)\mathbf{BC} + \mathbf{A}d\left(\mathbf{B}\right)\mathbf{C} + \mathbf{AB}d\left(\mathbf{C}\right)$, then leads to,

$$\mathrm{d}\mathbf{Y}_C = -\mathbf{Y}\mathbf{B}^T\mathrm{d}\left(\mathbf{B}\mathbf{Y}\mathbf{B}^T + \boldsymbol{\Gamma}\right)^{-1}\mathbf{B}\mathbf{Y}. \tag{51}$$

Recalling the differential of a matrix inverse, $\mathrm{d}\left(\mathbf{A}\right)^{-1} = -\mathbf{A}^{-1}\mathrm{d}\left(\mathbf{A}\right)\mathbf{A}^{-1}$ [56], yields

$$\mathrm{d}\mathbf{Y}_C = \mathbf{Y}\mathbf{B}^T\left(\mathbf{B}\mathbf{Y}\mathbf{B}^T + \boldsymbol{\Gamma}\right)^{-1}\mathrm{d}\left(\mathbf{B}\mathbf{Y}\mathbf{B}^T + \boldsymbol{\Gamma}\right)\left(\mathbf{B}\mathbf{Y}\mathbf{B}^T + \boldsymbol{\Gamma}\right)^{-1}\mathbf{B}\mathbf{Y} \tag{52}$$

which reduces to,

$$\mathrm{d}\mathbf{Y}_C = \mathbf{Y}\mathbf{B}^T\left(\mathbf{B}\mathbf{Y}\mathbf{B}^T + \boldsymbol{\Gamma}\right)^{-1}\mathrm{d}\left(\boldsymbol{\Gamma}\right)\left(\mathbf{B}\mathbf{Y}\mathbf{B}^T + \boldsymbol{\Gamma}\right)^{-1}\mathbf{B}\mathbf{Y}. \tag{53}$$

In Eq. (53), we can interpret $\mathrm{d}\mathbf{Y}_C$ as the small (complex) change in admittance, due to a small (complex) change in the interface flexibility $\mathrm{d}\left(\boldsymbol{\Gamma}\right)$. Importantly, $\mathrm{d}\left(\boldsymbol{\Gamma}\right)$ represents a small change in each matrix entry. Focusing attention on the nth interface connection in particular, such that $\mathrm{d}\left(\boldsymbol{\Gamma}\right) \rightarrow \mathbf{P}_n\mathrm{d}\gamma_n$, where $\mathbf{P}_n$ is a zero matrix bar the nth diagonal entry, whose value is one, Eq. (53) becomes,

$$\mathrm{d}\mathbf{Y}_C = \mathbf{Y}\mathbf{B}^T\left(\mathbf{B}\mathbf{Y}\mathbf{B}^T + \boldsymbol{\Gamma}\right)^{-1}\mathbf{P}_n\left(\mathbf{B}\mathbf{Y}\mathbf{B}^T + \boldsymbol{\Gamma}\right)^{-1}\mathbf{B}\mathbf{Y}\,\mathrm{d}\gamma_\mathrm{n} = \mathbf{J}_n\,\mathrm{d}\gamma_n \tag{54}$$

where $\mathrm{d}\gamma_n$ is a scalar differential of the nth interface flexibility, and $\mathbf{J}_n$ is a complex Jacobian matrix containing the partial derivatives of the coupled assembly admittance, with respect to the nth interface flexibility,

$$\mathbf{J}_n = \begin{bmatrix} \frac{\partial Y_{11}}{\partial \gamma_n} & \cdots & \frac{\partial Y_{1N}}{\partial \gamma_n} \\ \vdots & \ddots & \vdots \\ \frac{\partial Y_{N1}}{\partial \gamma_n} & \cdots & \frac{\partial Y_{NN}}{\partial \gamma_n} \end{bmatrix}. \tag{55}$$

Note that for a sufficiency small interface relaxation, the coupled admittance can be estimated according to,

$$\mathbf{Y}_C \approx \mathbf{Y}_C^{(\sim n)} + \Delta\mathbf{Y}_C^{(n)} = \mathbf{Y}_C^{(\sim n)} + \mathbf{J}_n\Delta\gamma_n \tag{56}$$

which represents a linear approximation of the assembly admittance, and is of similar form to Eq. (46).

To evaluate the Jacobian for a rigidly connected structure we set $\boldsymbol{\Gamma} = \mathbf{0}$. Its entries then describe the sensitivity of each assembly admittance to an infinitesimal relaxation of the nth interface. Note that Eq. (55) represents a matrix of *complex* derivatives. To provide a convenient single number descriptor for the admittance sensitivity with respect to the nth joint, it is convenient to consider the spatial average of the Jacobian's squared magnitude. Hence, we propose the following gradient-based sensitivity metric,

$$S_n^{(\mathrm{g})} = \frac{\left\langle \left|\mathbf{J}_n\right|^2 \right\rangle}{N} \tag{57}$$

where $\langle\square\rangle$ denotes the spatial average over a specified set of *target* DoFs, and N is chosen such that $S_1^{(\mathrm{g})} + S_2^{(\mathrm{g})} + \cdots + S_N^{(\mathrm{g})} = 1$.

The greater the value of $S_n^{(\mathrm{g})}$, the more sensitive the admittance matrix is (on average) to an infinitesimal relaxation of the nth interface.

5.2. Sample-based sensitivity

Among the global SA strategies available are a class of methods based on the use of a variance decomposition on the system's output [53]. A notable example being the Sobol indices [55].

Assuming a square integrable function $Y = f(\mathbf{X})$, the total variance in the output Y can be decomposed in the form [55],

$$V(Y) = \sum_i V_i + \sum_i \sum_{i>j} V_{ij} + \cdots + V_{i,j,\ldots,k} \tag{58}$$

where $V(\square)$ denotes the variance operator, and $V_{i,j,\ldots,k}$ represents a contribution to the output variance due to the input parameters $X_{i,j,\ldots,k}$. The decomposed variance terms are given by,

$$V_i = V_{X_i}(E_{\mathbf{X}_{\sim i}}(Y|X_i)) \tag{59}$$

$$V_{i,j} = V_{X_{ij}}(E_{\mathbf{X}_{\sim ij}}(Y|X_i, X_j)) - V_i - V_j \tag{60}$$

and so on, where $E(\square)$ denotes the expectation operator. T he term $E_{\mathbf{X}_{\sim n}}(Y|X_n)$ is read as, the expected value of the model output Y taken over all possible values of $\mathbf{X}_{\sim n}$, whilst keeping the input X_n fixed. The outer variance is then taken over all possible values of X_n.

According to above decomposition, the variance in the output of a model can be attributed to terms related to each input parameter (V_i), as well as the interaction effects between them ($V_{i,j,\ldots,k}$).

Normalising Eq. (58) by the total variance then yields,

$$\sum_i S_i + \sum_i \sum_{i>j} S_{ij} + \cdots + S_{i,j,\ldots,k} = 1. \tag{61}$$

The factors $S_{i,j,\ldots,k}$ describe sensitivity measures (Sobol indices) of increasing order. Of principal interest in most cases are the first order sensitivity measures, defined as,

$$S_n = \frac{V_{X_n}(E_{\mathbf{X}_{\sim n}}(Y|X_n))}{V(Y)}. \tag{62}$$

Note that S_n is a normalised metric, as $V_{X_n}(E_{\mathbf{X}_{\sim n}}(Y|X_n))$ varies between zero and $V(Y)$. It provides a measure of the sensitivity of the model output to the input X_n alone; it neglects the influence of any interaction between X_n and the remaining inputs $\mathbf{X}_{\sim n}$.

Another related metric is that of the total effect index, given by,

$$S_{Tn} = 1 - \frac{V_{\mathbf{X}_{\sim n}}(E_{X_n}(Y|\mathbf{X}_{\sim n}))}{V(Y)}. \tag{63}$$

Here, the term $V_{\mathbf{X}_{\sim n}}(E_{X_n}(Y|\mathbf{X}_{\sim n}))$ describes the first order effect due to all input parameters $\mathbf{X}_{\sim n}$ bar X_n. Hence, $V(Y) - V_{\mathbf{X}_{\sim n}}(E_{X_n}(Y|\mathbf{X}_{\sim n}))$ describes the contribution of all terms in the variance decomposition which include X_n. The total effect index thus describes the influence of the input parameter X_n, along with the effect of its interaction with all other inputs. For details on the numerical estimation of the Sobol indices the reader is referred to [57] (see Table 2 for necessary formulas).

To develop a global identification of response-critical joints we consider a model of the form,

$$Y = \left\langle |\mathbf{Y}_C|^2 \right\rangle = f(k_1, r_1, k_2, r_2, \ldots, k_N, r_N) = f(\mathbf{X}) \tag{64}$$

and compute the total effect index for each joint. To enable fair comparison against gradient and interval-based metrics, each index is normalised,

$$S_n^{(s)} = \frac{S_{Tn}}{N} \tag{65}$$

such that $S_1^{(s)} + S_2^{(s)} + \cdots + S_N^{(s)} = 1$, where the superscript $\square^{(s)}$ is used to indicate that this is a sample-based sensitivity metric. These are then rank ordered to identify the response-critical joints. The greater the value of $S_n^{(s)}$, the greater the amount of output variance that can be attributed to the relaxation of the nth interface.

To aid a fair comparison when using the sample-based metric $S_n^{(s)}$, the range of permissible stiffness and damping values (k_n, r_n) should be the same for each joint. A principal advantage of the global method is that the interaction between several joints can be accounted for; the gradient-based metric presented above, and the interval-based metric presented below, consider only a single joint at a time. This advantage is, however, offset by the computational effort required to compute numerically the sample-based metric.

5.3. Interval-based sensitivity

The local and global methods described above are limited, respectively, by the assumption of linearity and computational efficiency. Herein we propose an interval-based identification that overcomes both these limitations. Whilst the interval-based approach does not provide a detailed analysis like the global approach, it avoids the need to sample the entire input space to identify the response-critical joints; instead of treating each input as a distribution, intervals are considered and the bounds of the output are determined analytically. These bounds will form the basis of the proposed interval-based sensitivity metric $S_n^{(i)}$.

The general concept of interval-based sensitivity analysis was first introduced in [58], where the authors considered the change in absolute interval widths on the input (x) and the output (y) side of the problem. Their proposed sensitivity metric takes the form,

$$S = \frac{\partial(\overline{y} - \underline{y})}{\partial(\overline{x} - \underline{x})}. \tag{66}$$

The authors present a numerical example whereby the frequency response function of a lumped parameter truck model is subject to an interval sensitivity analysis with respect to its lumped mass values. In the present paper we are interested in the sensitivity of a scalar output quantity (the spatially averaged magnitude squared admittance) to a *complex pair* of input intervals (joint stiffness and damping) whose maxima extend to ∞. For this specific case we propose an alternative metric, described below.

Recalling the interval matrix of Eq. (45), with consideration of Eq. (54), we have,

$$\{\Delta \mathbf{Y}_C^{(n)}\} = \{w_n\} \otimes \mathbf{Y}\mathbf{B}^T \left(\mathbf{B}\mathbf{Y}\mathbf{B}^T + \mathbf{\Gamma}^{(-n)}\right)^{-1} \mathbf{P}_n \left(\mathbf{B}\mathbf{Y}\mathbf{B}^T + \mathbf{\Gamma}^{(-n)}\right)^{-1} \mathbf{B}\mathbf{Y} = \mathbf{J}_n \otimes \{w_n\} \tag{67}$$

Table 1
System parameters used in numerical mass–spring example, and natural frequencies obtained for rigid coupling.

Index	1	2	3	4	5	6	7	8	9	10	11
$m_\square$ (kg)	1	0.5	1.2	0.65	0.9	0.56	1.2	0.52	1.1	0.25	1.5
$k_\square \times 10^4$ (N/m)	2	3	1	4	0.5	1	2	2	3	1	0.8
$c_\square$ (Ns/m)	1	1	1	1	1	1	1	1	1	1	1
$f_\square$ (Hz)	7.3	14.9	18.6	21.8	34.3	38.2	68.3	73.5	–	–	–

Note that unlike $\mathbf{J}_n \Delta\gamma_n$, which describes a linearised joint contribution, the interval $\mathbf{J}_n \otimes \{w_n\}$ represents the upper and lower bounds for an arbitrary relaxation of the interface. Hence, it takes into account the non-linearities that arise due to the matrix inversion (see Eq. (43)). Considering the upper and lower bounds of the complex interval $\{\Delta\mathbf{Y}_C^{(n)}\}$, we define the interval-based sensitivity metric,

$$S_n^{(i)} = \frac{\left\langle \text{real}\left(\Delta\overline{\mathbf{Y}}_C^{(n)}\right) - \text{real}\left(\Delta\underline{\mathbf{Y}}_C^{(n)}\right)\right\rangle^2 + \left\langle \text{imag}\left(\Delta\overline{\mathbf{Y}}_C^{(n)}\right) - \text{imag}\left(\Delta\underline{\mathbf{Y}}_C^{(n)}\right)\right\rangle^2}{N} \tag{68}$$

where, as before, N is chosen such that $S_1^{(i)} + S_2^{(i)} + \cdots + S_N^{(i)} = 1$. The numerator of Eq. (68) may be interpreted as an (average) measure of the size of the complex interval $\{\Delta\mathbf{Y}_C^{(n)}\}$; recalling that a complex interval describes a rectangle in the complex plane, $S_n^{(i)}$ represents the normalised squared distance across the diagonal of said rectangle.[1] Hence, the greater the value of $S_n^{(i)}$, the greater the size of the output interval.

Unlike the metric proposed in [58], we consider only the interval bound of the output (as the input bound extends to infinity). To aid a fair comparison when using the interval-based metric $S_n^{(i)}$, each $\{\Delta\mathbf{Y}_C^{(n)}\}$ should be determined subject to the same joint interval bounds $\{Z_n\}$.

For a sufficiently large lower stiffness bound $\underline{Z}_n$, we would expect $S_n^{(i)}$ to follow the same trend as $S_n^{(g)}$, as $\{z_n\} = \{Z_n\} \oplus \text{tr}\left(\mathbf{P}_n\mathbf{A}^{-1}\right)$ would be dominated by the joint stiffness $\{Z_n\}$, and so $\{w\} \approx 1 \oslash \{Z_n\} = \{\gamma_n\}$ would appear simply as a scaling factor. Treating the interface stiffness as a non-interval parameter, such that $\{\gamma_n\} \to \Delta\gamma_n$, this would be equivalent to the linearised estimation of the coupled assembly admittance (Eq. (56)).

6. Numerical example

In this section we present two numerical examples demonstrating the interval assessment of joint variability and the identification of response-critical joints, the first a simple mass–spring system and the latter a more representative Finite Element (FE) frame assembly.

6.1. A simple mass–spring system

The system considered in this initial example is illustrated in Fig. 3. It is an 11 DoF mass–spring–damper system. It constitutes two sub-systems (green and blue) connected by 3 joint elements (red). System parameters are given in Table 1, and were chosen arbitrarily to obtain suitably spaced resonances between 1 to 200 Hz. Each joint element is characterised by its flexibility γ_n, or equivalently its dynamic stiffness Z_n. We are interested in a) obtaining the interval bounds of the coupled admittance matrix $\mathbf{Y}_C$, and b) identifying the response-critical joints, i.e. determining, at each frequency, which joint contributes most to the dynamics of the assembled system.

6.1.1. Interval-based joint variability

We begin by considering the interval bounds of the coupled admittance based on the interval representation of a particular joint; joint 1 is described by the complex interval $\{Z_1\} = \{k\} + i\{r\} = [\underline{k} \quad \infty] + i[\underline{r} \quad \infty]$ whilst joints 2 and 3 are taken to be rigid ($\gamma_2 = \gamma_3 = 0$). Hence, the interval admittance matrix should describe the entire range of possible admittance values given any combination of joint stiffness and damping that is made permissible by the interval $\{Z_1\}$. Note that the upper bounds of the joint interval represent a rigid connection.

The complex admittance interval $\{\mathbf{Y}_C\}$ is determined as per Eq. (45),

$$\{\mathbf{Y}_C\} = \mathbf{Y} - \mathbf{Y}\mathbf{B}^T\left(\mathbf{B}\mathbf{Y}\mathbf{B}^T + \mathbf{\Gamma}^{(\sim n)}\right)^{-1}\mathbf{B}\mathbf{Y} \oplus \left[\{w_n\} \otimes \mathbf{Y}\mathbf{B}^T\left(\mathbf{B}\mathbf{Y}\mathbf{B}^T + \mathbf{\Gamma}^{(\sim n)}\right)^{-1}\mathbf{P}_n\left(\mathbf{B}\mathbf{Y}\mathbf{B}^T + \mathbf{\Gamma}^{(\sim n)}\right)^{-1}\mathbf{B}\mathbf{Y}\right]$$

where

$$\{w_n\} = 1 \oslash \left[\{Z_n\} \oplus \text{tr}\left(\mathbf{P}_n\mathbf{A}^{-1}\right)\right] = 1 \oslash \{z_n\} \tag{69}$$

[1] An alternative metric could be formulated by instead considering the (average) *area* of the complex interval,

$$S_n^{(i)} = \left\langle \text{real}\left(\Delta\overline{\mathbf{Y}}_C^{(n)}\right) - \text{real}\left(\Delta\underline{\mathbf{Y}}_C^{(n)}\right)\right\rangle \left\langle \text{imag}\left(\Delta\overline{\mathbf{Y}}_C^{(n)}\right) - \text{imag}\left(\Delta\underline{\mathbf{Y}}_C^{(n)}\right)\right\rangle / N.$$

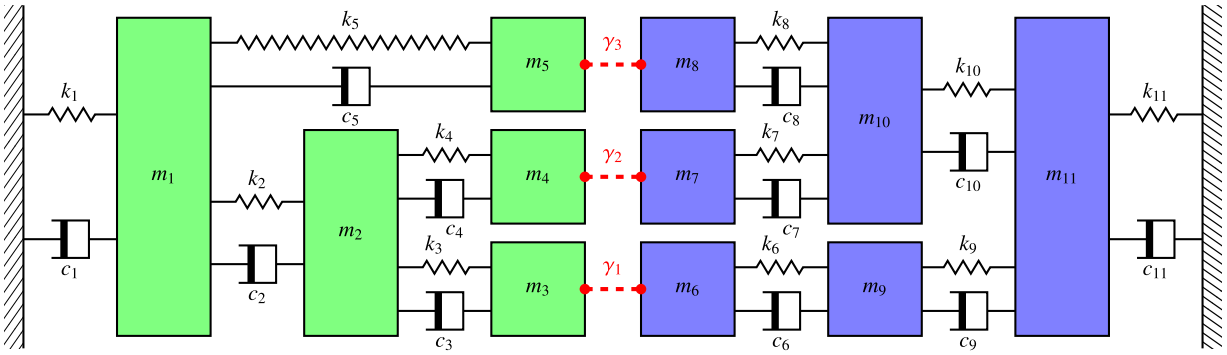

Fig. 3. Numerical mass–spring example. System parameters are given in Table 1 along with the natural frequencies for the rigidly coupled case. (For interpretation of the references to colour in this figure legend, the reader is referred to the web version of this article.)

is a complex interval to be determined. Using the approach outlined in Appendix A (see Algorithm 1), alongside the interval arithmetic described in Section 2, the complex reciprocal interval $\{w_n\}$ can be determined straightforwardly.

Shown in Fig. 4 are the upper and lower bounds of the real (b) and imaginary (c) parts of $\{w_n\}$ according to the joint interval $\{Z_1\} = [100 \quad \infty] + i\,[100 \quad \infty]$. The dashed blue curves indicate the interval computation, whilst the orange curves show the max/min values obtained using a sampling-based estimation, where 40 000 combinations of k and r are considered. Shown in Fig. 4a are the lower bounds of the complex interval $\{z_n\}$ used to compute $\{w\}$ (note that the upper bounds are ∞, representing a rigid connection). It is clear from Fig. 4bc that a particular combination of joint stiffness and damping will yield a w with a particular set of peaks, and by uniform sampling we obtain a series of such. Gaps between successive peaks are a result of the discrete sampling employed and represent a limitation of such a sample-based estimation. That is not to say that the sample based estimate is inaccurate, rather it requires a greater computational effort to achieve a result similar to that of the interval computation, which, as expected, encloses the max/min values of all samples drawn. The results of Fig. 4 demonstrate the application and validity of the conformal mapping approach discussed in Appendix A.

Implementation of Eq. (45), taking into account the appropriate interval arithmetic, then yields a complex interval for the coupled admittance. Shown in Fig. 5a and b are, respectively, the real and imaginary interval bounds of the transfer admittance $Y_{1,11}$. Dashed blue curves were obtained by the interval method described above, whilst orange curves were obtained by sampling. Shown in Fig. 6 is the magnitude transfer admittance $|Y_{1,11}|$ of the rigidly coupled assembly (black) alongside the maximum interval bound (blue) obtained from the real and imaginary intervals presented in Fig. 5. Also shown in orange is the result obtained by sampling. The interval computation can be seen to encapsulate entirely the sample estimate. This maximum bound represents the maximum attainable admittance based on the relaxation of interface 1 in Fig. 6. It does not, however, provide any indication as to the most likely outcome, as per the possibilistic paradigm.

Note that the lower bound in Fig. 6 has been omitted. The reason for doing so is that in computing the interval of the magnitude admittance, the real and imaginary parts must each be squared. If both parts have a lower bound less than zero *and* an upper bound greater than zero (i.e. zero is enclosed within the bound), their squared intervals must have a lower bound of zero. Hence, their sum also has a lower bound of 0, so it cannot be presented on a logarithmic scale. Nevertheless, Fig. 6 demonstrates that the proposed interval assessment of joint variability is able to provide an upper limit on the possible admittance. This is, of course, for a single joint. The interval assessment of multiple joints simultaneously would require a non-trivial extension of the method proposed herein.

Shown in Fig. 7 are the upper interval bounds obtained by relaxing each interface individually according to the interval stiffness, $\{Z_n\} = [100 \quad \infty] + i\,[100 \quad \infty]$. The upper bounds provide a visual indication of which interface joint has the greatest *possible* influence on the coupled transfer admittance $|Y_{1,11}|$. As expected, the relative importance of each joint varies with frequency. A more intuitive presentation of this result is obtained by considering the sensitivity metrics proposed in Section 5. These will be shown in following sub-section.

Shown in Fig. 8 are the upper and lower bounds of the magnitude transfer admittance $|Y_{1,11}|$ obtained by successively increasing the minimum bound of the joint stiffness and damping, such that $\{Z_n\} = [\underline{Z} \quad \infty] + i\,[\underline{Z} \quad \infty]$, where $\underline{Z} = [100, 1000, 10000, 100000]$. As mentioned previously, if the complex interval $\{Y_C\}$ contains the origin, then the lower bound of its squared magnitude will always be zero. This occurs frequently for large joint intervals. As the origin is always contained within the interval $\{w_n\}$ (see Fig. A.14), the bounds of $\left\{\Delta\mathbf{Y}_C^{(n)}\right\}$ also contains the origin (since complex multiplication can be interpreted as a rotation followed by a scaling). The subsequent addition, $\mathbf{Y}_C^{(\sim n)} \oplus \left\{\Delta\mathbf{Y}_C^{(n)}\right\}$, translates the bound. To avoid enclosing the origin, this translation must occur in the appropriate direction. Had the upper bounds of $\{Z_n\}$ been considered finite, the origin would not be enclosed by $\{w_n\}$, and a more useful lower bound obtained.

From Fig. 8 it can be observed that the interval bounds are not simply scaled for increasing relaxation; new characteristics emerge as the joint is made more flexible. These flexibility dependent characteristics are neglected when considering a gradient-based estimation of the coupled admittance, as per Eq. (56).

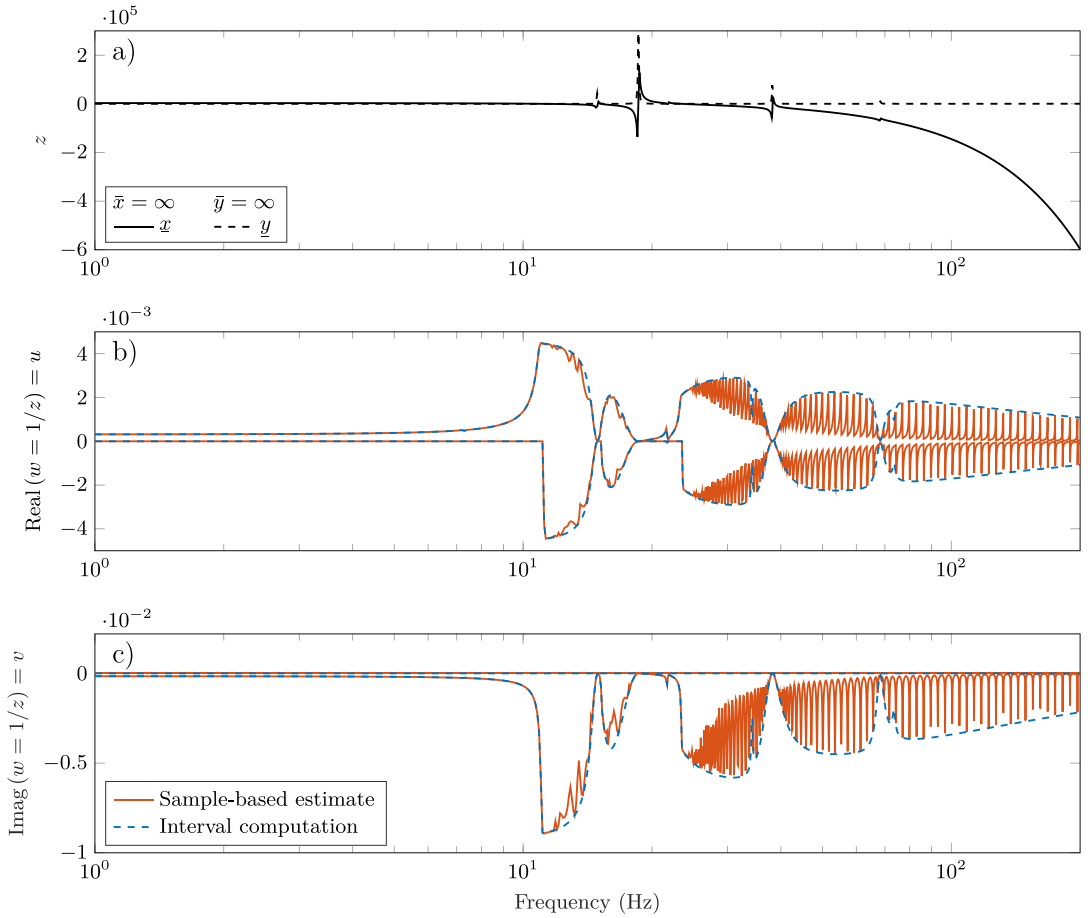

Fig. 4. Interval computation for numerical example. a) Lower bounds of the complex interval $\{z_n\} = \{x_n\} + i\{y_n\}$. b/c) Upper and lower bounds of the real/imaginary parts of the complex interval $\{w_n\} = 1 \oslash \{z_n\}$: blue dashed lines are interval computations, orange lines are sample-based estimates.

6.1.2. *Response-critical joint identification*

To identify the response-critical joints of an assembly it is necessary to compare their influence on the dynamics of the assembled structure. In Section 5 we proposed three sensitivity metrics to do so. In this section we apply those metrics to the numerical example of Fig. 3. We consider two cases: $\underline{Z}_n = 1 \times 10^8(1+i)$ and $\underline{Z}_n = 100(1+i)$, representing a minor and major relaxation of the interface, respectively.

The interval and gradient-based metrics, $S_n^{(i)}$ and $S_n^{(g)}$, are computed analytically according to Sections 5.1 and 5.3 (making sure to adopt interval arithmetic for the former), taking mass 11 to be the target DoF. The sample-based metric $S_n^{(s)}$ is computed numerically by sampling over the input parameter space. For the example considered, the input space consists of 6 parameters, the stiffness and damping of each joint. At each frequency, 2000 samples were drawn between $\underline{Z}_n$ and $\underline{Z}_n \times 10^7$ (representing an approx. rigid connection). Samples were distributed such that each parameter's logarithm was uniformly distributed between the specified bounds.

Shown in Fig. 9a and 9b are the sensitivity metrics obtained for the two cases considered (top — interval-based, middle — gradient-based, bottom — sample-based). The results of Fig. 9a represent the minor relaxation of the interface, and Fig. 9b the major. Considering first Fig. 9a, it is clear that we get significant agreement between all three metrics (to be expected for a minor relaxation). We observe that at low frequencies, joints 1 (blue) and 2 (yellow) dominate the response, whilst at high frequencies, joint 3 (purple) becomes the key contributor. Across the middle range joint 2 tends to dominate, with joints 1 and 3 contributing across narrow frequency ranges.

Let us now consider Fig. 9b, representing the major interface relaxation. Note that the gradient-based metric is unchanged, as it does not depend on the level of relaxation. Whilst the interval and gradient-based metrics share some similar trends, it is clear that across the middle frequency range some discrepancies have emerged. These differences are due to the non-linear contribution of each joint's flexibility (as observed in Fig. 8). Importantly, this suggests that the possible influence, or importance, of a joint depends on the range of permissible stiffness and damping values that can be taken.

The sampling-based metric $S_n^{(s)}$ is harder to interpret. The issue is that given the range of stiffness/damping values permissible, a large range of assembly responses are observed. This can cause numerical issues when estimating the Sobol indices. Furthermore,

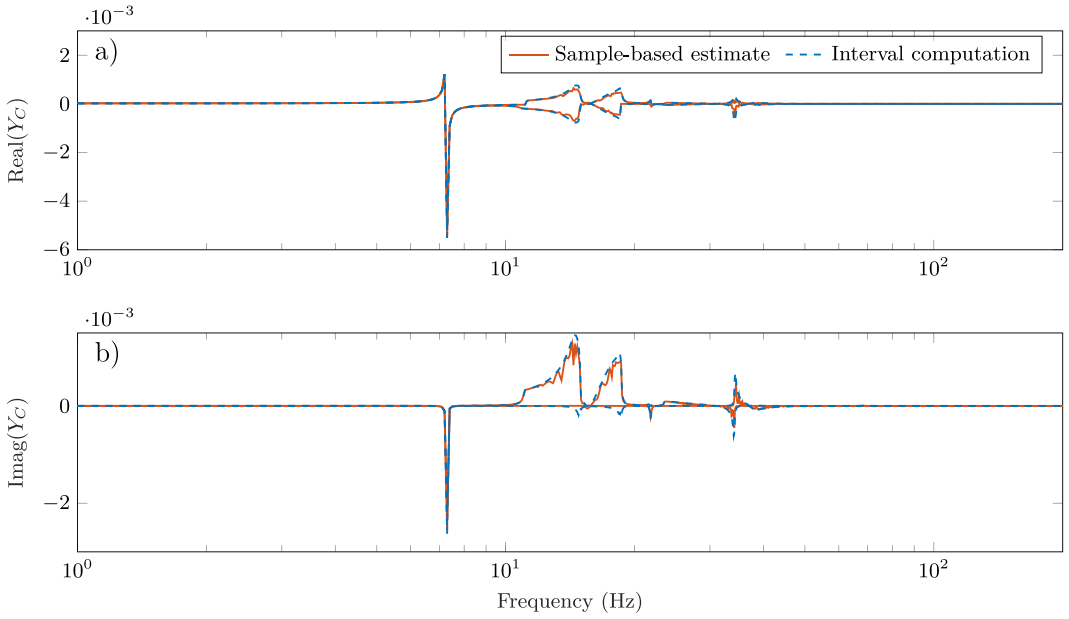

Fig. 5. Real (a) and imaginary (b) interval bounds of the admittance $Y_{1,11}$ due to relaxation of joint interface: blue lines are interval computations, orange lines are sample-based estimates.

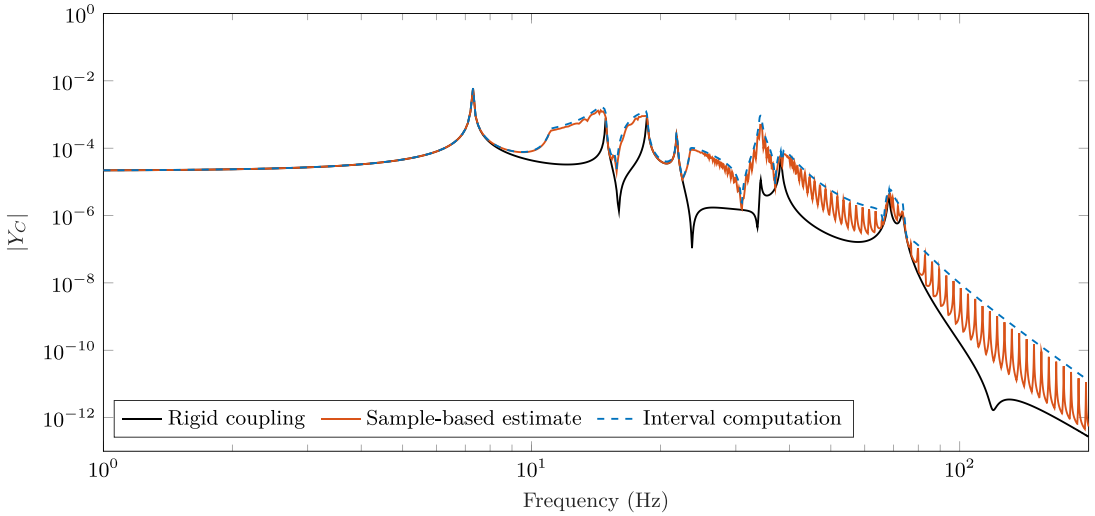

Fig. 6. Upper bound of the magnitude admittance $|Y_{1,11}|$ due to relaxation of the joint interface: blue lines are interval computations, orange lines are sample-based estimates. Lower bounds are omitted for clarity. (For interpretation of the references to colour in this figure legend, the reader is referred to the web version of this article.)

as suggested by Fig. 6, at high frequencies a uniform sampling scheme leads to a series of peaks in the response bound. These peaks cause rapid fluctuations in the obtained Sobol indices, complicating their interpretation. This issue could be alleviated by increasing the number of samples drawn to more suitably cover the entire input space. This would of course come at the cost of additional computational effort. This is the principal limitation of the sample-based approach. It is also worth noting that the interval-based metric considers the entire range of possible assembly responses, no matter how unlikely the extreme values are. The sample-based metric, on the other hand, considers the spread, or variance, of outcomes, so will be less influenced by unlikely extremum values. For example, the sample-based metric does not indicate an increase in sensitivity due to joint 1 around 80–90 Hz, whilst the interval-based metric does. This is likely due to the small range of input stiffness/damping values that cause this increased sensitivity. These particular values are likely missed by the sample-based approach, or their influence is outweighed by regions of

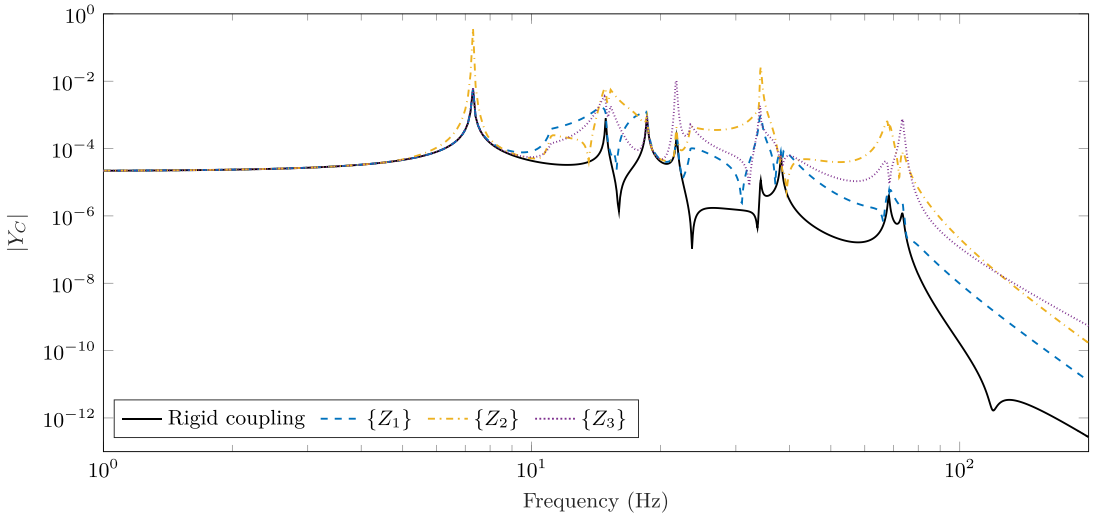

Fig. 7. Comparison of the upper bound on $|Y_{1,11}|$ due the relaxation of each interface joint such that $\{Z_n\} = [100 \quad \infty] + i\,[100 \quad \infty]$. Rigid coupling is shown in black. Lower bounds are omitted for clarity.

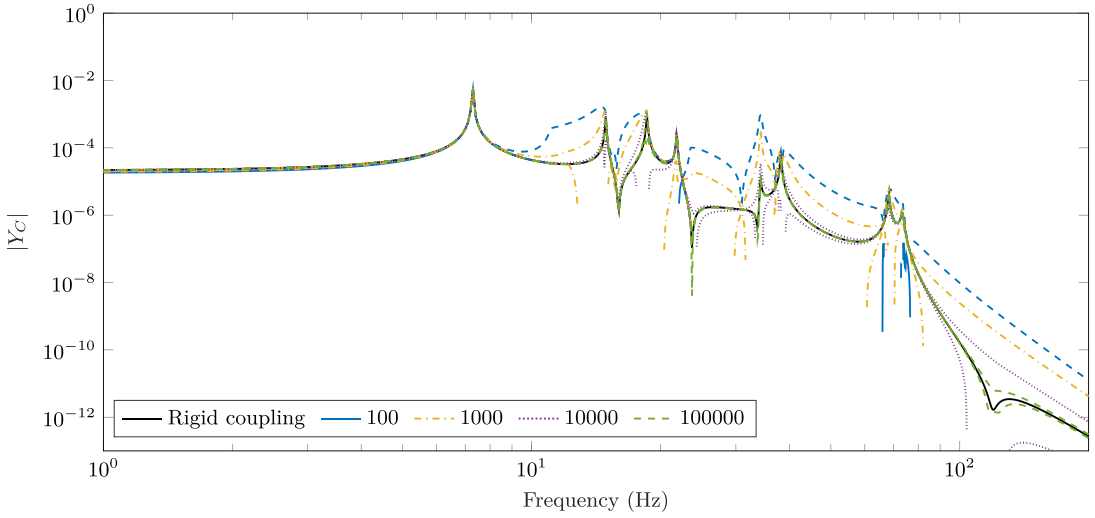

Fig. 8. Comparison of the upper and lower bounds on $|Y_{1,11}|$ due an increasing relaxation of the interface joint, $\{Z_n\} = [\underline{Z} \quad \infty] + i\,[\underline{Z} \quad \infty]$ where $\underline{Z} = [100, 1000, 10000, 100000]$.

the output space that are more densely populated. Nevertheless, noticeable differences are observed between Fig. 9a and b, inline with the results of the interval-based metric.

The results of Fig. 9b are supported by the upper interval bounds shown in Fig. 7, where it can be seen that, in general, the greater the upper bound of the magnitude transfer admittance, the greater the sensitivity metric.

Whilst it may be argued that the sampling-based metric $S_n^{(s)}$ will likely provide a more robust analysis, being less sensitive to unlikely outcomes, this comes at the cost of considerable computational effort, especially for large levels of relaxation. For the mass–spring example considered (running on a standard desktop machine with an Intel(R) Core(TM) i7-8700 CPU 3.20 GHz and 16 GB RAM, over 2000 frequency points), the metric computation times were as follows: gradient-based — 0.155 s; interval-based — 0.424 s; sampling-based — 600.9 s. Note that the sampling-based metric involves the repeated sampling of 2000 log-uniformly distributed values assigned to each of the 6 joint parameters (i.e. stiffness and damping of each joint), and that is done at every frequency point, hence its rather large computation time. Furthermore, without detailed statistical information of the joint, such a method is somewhat unwarranted. Computation of the interval-based metric, on the other hand, is of the order of the gradient-based metric, and does not require any detailed statistical information.

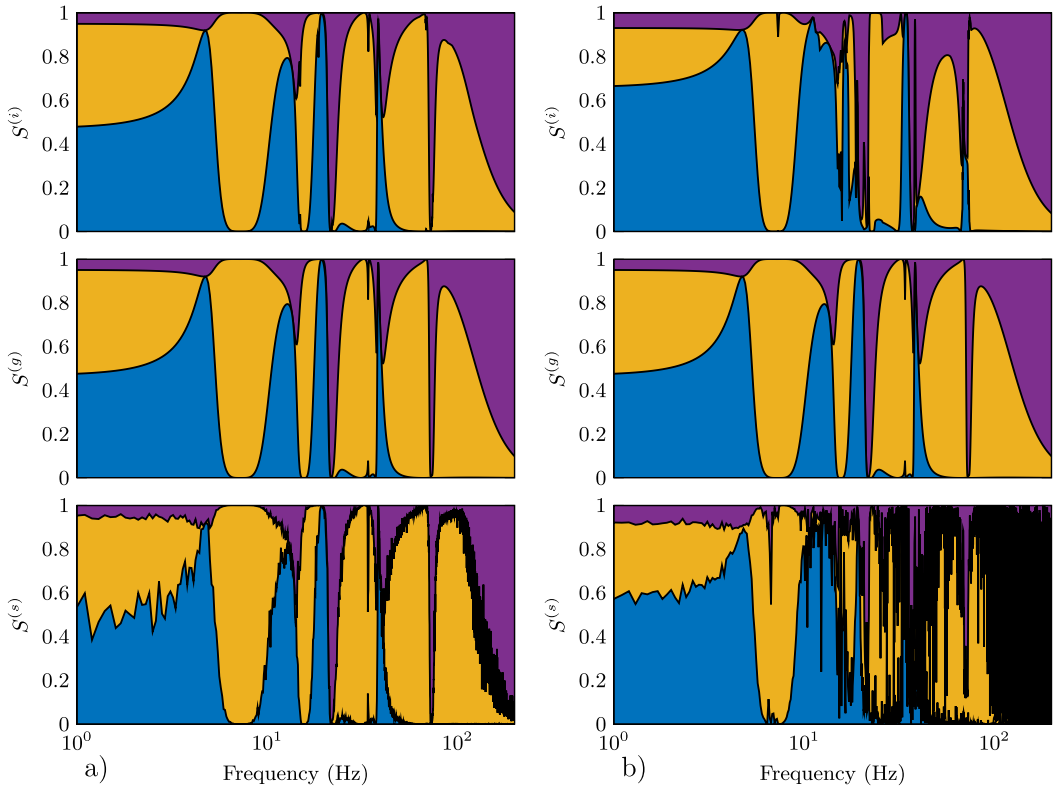

Fig. 9. Comparison of the interval (top), gradient (middle), and sample-based (bottom) sensitivity metrics for the minimum stiffness bounds $\underline{Z}_n = 1 \times 10^8(1+i)$ (a) and $\underline{Z}_n = 100(1+i)$ (b): $S_1^{(\square)}$ - blue, $S_2^{(\square)}$ - yellow, $S_3^{(\square)}$ - purple. (For interpretation of the references to colour in this figure legend, the reader is referred to the web version of this article.)

6.2. A more practical, albeit numerical, example

In this section we will demonstrate the identification of response-critical joints on a more representative numerical assembly. The chosen assembly consists of two frame-like components coupled together at four locations, as illustrated in Fig. 10. At each connection, coupling is enforced through 4 translational links in the vertical z direction; for simplicity in-plane coupling is neglected. Through an appropriate interface transformation, each 4 link connection can be characterised by a single translational coupling, with two accompanying rotations, yielding a total of 12 interface DoFs. A further remote DoF is included on each component.

The question to be answered is as follows: given limited experimental and/or numerical resources, which interface connection (c_1, c_2, c_3, or c_4; starting from the connection closest to the origin and moving clockwise) should be treated as a flexible joint, characterised, and implemented numerically to aid model refinement? In what follows we will use the gradient and interval-based sensitivity metrics proposed through Section 5 to identify the response-critical joints and answer this question.

The assembly is modelled using the FE method, implemented in MATLAB using the PDE Toolbox [59]. Both frames are specified as steel with structural loss factor $\eta = 0.025$. Shown in Fig. 11 are some example mode shapes of the rigidly coupled assembly. After solving the eigen-problem for each frame, the free interface admittance matrices $\mathbf{Y}_A$ and $\mathbf{Y}_B$ are determined by modal summation and a finite difference transformation is used to obtain the sought after translational/rotational admittances at each connection [60]. These form the inputs to the gradient and interval-based sensitivity analyses.

As before, we consider two cases with different levels of interface relaxation. In the first each joint is described in turn by the interval $\{Z_n\} = [1 \times 10^8 \quad \infty] + i[1 \times 10^8 \quad \infty]$, representing a minor relaxation of the interface. In the second, we set $\{Z_n\} = [1 \times 10^5 \quad \infty] + i[1 \times 10^5 \quad \infty]$, representing a moderate relaxation of the interface. For each case we employ the gradient and interval-based sensitivity metrics described in Sections 5.1 and 5.3, respectively. Owing to its computational effort and poor performance, the sampling-based Sobol metric is not considered here. Results are presented in Fig. 12 with left and right-hand side plots representing the minor and moderate relaxations, respectively. Middle and bottom plots show, respectively, the interval and gradient-based sensitivity metrics for each connection.

Note that the metrics presented describe the contribution of the entire connection, including both translational and rotational DoFs. To obtain these results the sensitivity metrics for each DoF are summed together. For example, the combined metric for

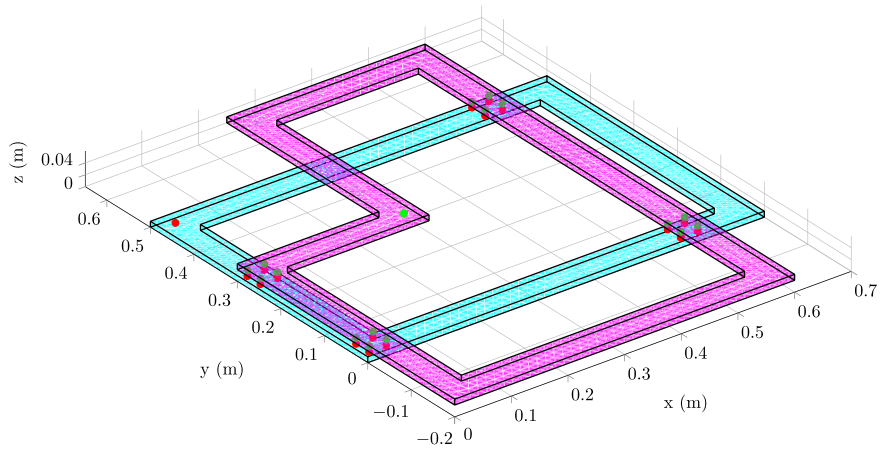

Fig. 10. Diagram of numerical example. Two frame structures coupled at 4 locations (c_1, c_2, c_3, and c_4, located clockwise from the origin), each with 4 translational z DoFs.

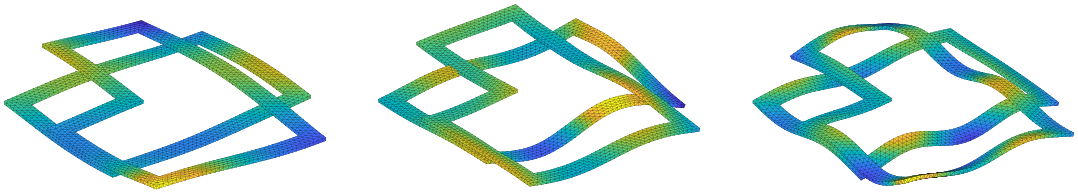

Fig. 11. Some example mode shapes of coupled structure.

connection 1 is given by,

$$S_1^{(\square)} = S_{11}^{(\square)} + S_{12}^{(\square)} + S_{13}^{(\square)} \tag{70}$$

where $S_{11}^{(\square)}$, $S_{12}^{(\square)}$, and $S_{13}^{(\square)}$ are the sensitivity metrics for the translational and x/y rotational DoFs at connection 1. Using this approach one could similarly compare the importance of different DoFs (e.g. translational vs. rotational), as opposed to connection points.

Shown in the top plots of Fig. 12 are the remote DoF transfer admittances for the rigidly coupled assembly (black), and those obtained by independently relaxing the DoFs at each connection by an amount equal to the minimal stiffness bound $\underline{Z}_n$. These plots provide an indication of the sensitivity of the transfer admittance given the relaxation of each interface connection. They do not, however, provide an insight into the range of possible outcomes. Nevertheless, we can use them to help interpret the sensitivity metrics displayed beneath.

As before, for a minor relaxation the gradient and interval-based metrics display the same general trends. For the moderate relaxation clear differences can be seen. This again illustrates the importance of considering the entire range of possible stiffness and damping values when determining the influence of specific joint. For a minor relaxation, in the low-mid frequency range (100–350 Hz), both metrics indicate that the connection 3 has the greatest influence, with connection 4 contributing significantly over narrower frequency ranges. At higher frequencies (> 350 Hz) the influence of connection 2 increases markedly. For the moderate relaxation, according to the interval-based metric, the influence of connections 3 and 4 reduce considerably compared to Fig. 12a, particularity around 200 Hz, with connection 2 becoming dominant. It is further observed that in the mid-high frequency range (> 200 Hz) the influence of connection 1 increases, and at some frequencies becomes dominant.

Comparing the interval-based metrics for the moderate relaxation (middle right plot) with their respective transfer admittances (top right plot) it can be seen that regions of increased sensitivity generally correspond to greater deviations from the rigid admittance (in black). Though, this is not always the case. It is important to recall that the interval-based metric considers the range of all possible transfer admittances given the permissible joint dynamics. The transfer admittances plotted are those obtained for $Z_n = 1 \times 10^8 + i\,1 \times 10^8$ alone, which is just one realisation.

The information provided by the proposed sensitivity metrics could be used to guide model refinement. As an example, from Fig. 12 it is clear that connection 1 has the least influence overall, hence efforts should not be focused towards refinement of this

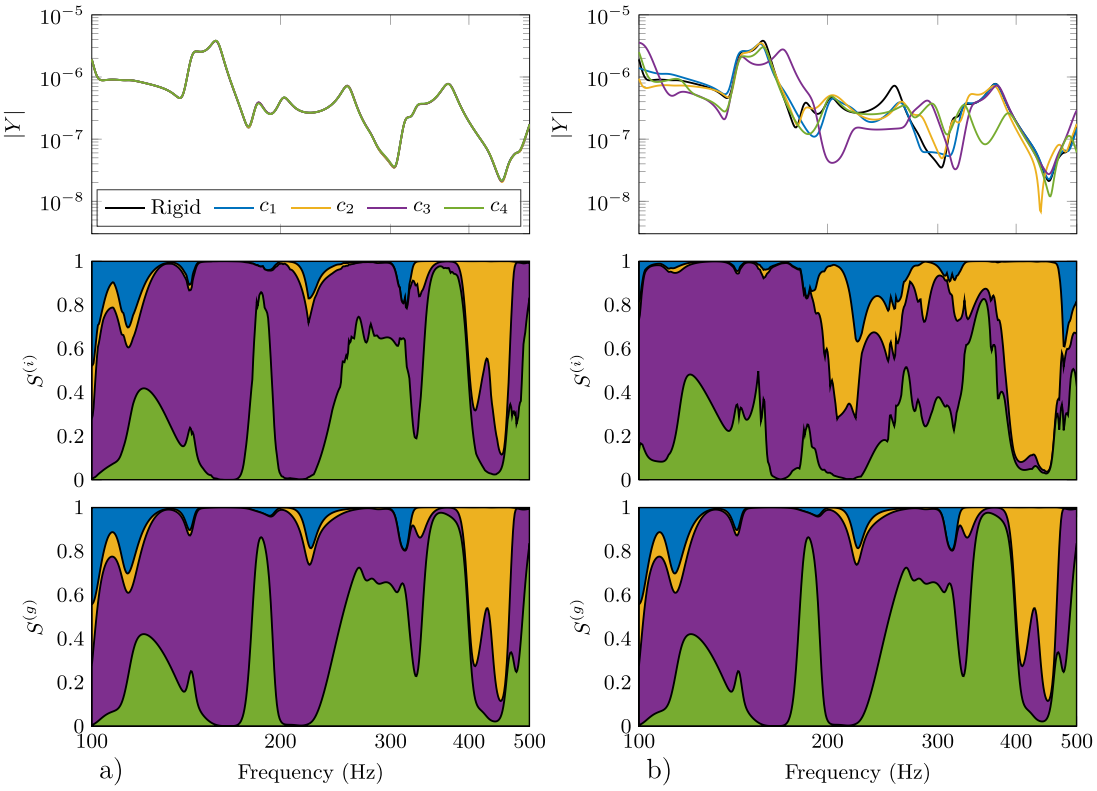

Fig. 12. Comparison of the interval (middle) and gradient (bottom) based sensitivity metrics for minimum stiffness bounds $\underline{Z}_n = 1 \times 10^8(1+i)$ (a) and $\underline{Z}_n = 1 \times 10^5(1+i)$ (b). Each metric describes the sensitivity of the transfer admittance with respect to a specific connection point, including both its translational and rotational DoFs: $S_1^{(\square)}$ - blue, $S_2^{(\square)}$ - yellow, $S_3^{(\square)}$ - purple, $S_4^{(\square)}$ - green. Shown in the top figures are the transfer admittances obtained by independently relaxing the DoFs at each connection point by an amount equal to the minimal stiffness bound. In black is the response obtained from the rigid assembly. (For interpretation of the references to colour in this figure legend, the reader is referred to the web version of this article.)

particular connection. In the low frequency range connection 3 has the greatest influence and should be prioritised. If attention is focused on the mid frequency range connection 4 might be prioritised instead.

7. Conclusions

Whilst there exists a large body of literature related to the characterisation and modelling of joint dynamics, it appears few works have considered *which* joints to characterise and/or model; for a complex built-up structure the number of joints present may prohibit the complete characterisation/modelling of all joints. With the development or refinement of a component-based model there is a need to identify the *response-critical joints* of an assembly — those that have the greatest influence on the target response. Once identified, experimental and computational resources may be focused towards those joints which will benefit the modelling effort most. In the present paper a possibilistic interval-based sensitivity metric is proposed to rank order the influence of individual joints towards the dynamics of an assembled structure.

The interval-based sensitivity metric was formulated by exploiting the Sherman–Morrison formula and the dual sub-structuring formulation. A complex interval representation was adopted for the interface stiffness/damping, and the complex interval bounds of the assembled admittance matrix (also operational response) were obtained. Spatial averaging of the admittance interval bounds over selected DoFs yield the proposed metric. Scaled between 0 and 1 the metric represents a normalised measure of the size of the complex output interval, and enables a clear identification of the assembly's response-critical joints.

The advantages of an interval-based sensitivity metric, over a more conventional probabilistic one, are two fold: no detailed statistical information is required to describe the joint parameters (only a minimum bound for the stiffness and damping), and computationally expensive sampling methods are avoided. Furthermore, the interval-based approach, whilst providing only the extremum outcomes, considers the entire input space and so implicitly takes into account model non-linearity (hence we term the method 'pseudo-global'). This is in contrast to typical gradient-based methods which assume linearity and/or small input variance.

As part of a numerical example, the proposed metric was compared against local gradient-based and global sampling-based (Sobol) metrics, also proposed herein. For low levels of interface relaxation, all metrics are in strong agreement. For larger levels of relaxation, the influence of model non-linearity is observed and the interval/sampling-based metrics differ from the gradient-based.

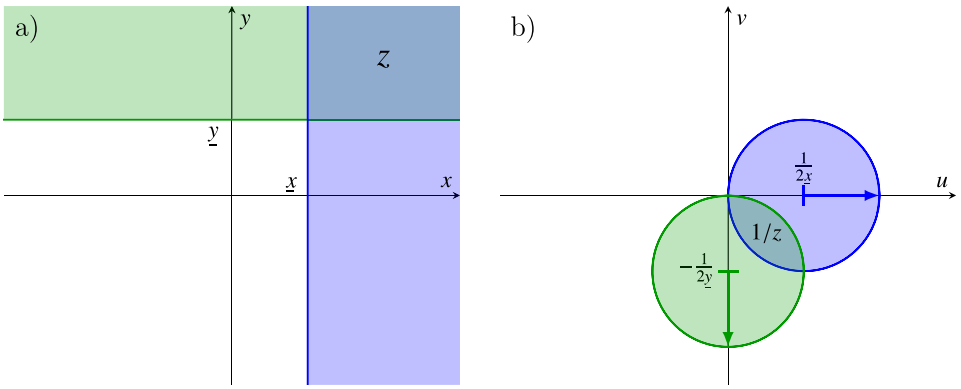

Fig. A.13. Conformal map $f(z) = 1/z$ applied to the open regions $x > \underline{x}$ (blue) and $y > \underline{y}$ (green). (For interpretation of the references to colour in this figure legend, the reader is referred to the web version of this article.)

This result demonsrates that the relative importance of a joint depends on the range of permissible stiffness and damping values that can be taken. Owing to numerical and finite sampling issues, the global metric performs poorly at high frequencies where there is large variance in the model output. For this reason the sample-based metric is considered the least beneficial. In contrast, both gradient and interval-based metrics are computed analytically, and so avoid such issues. Nevertheless, whilst the gradient-based metric avoids costly sampling efforts, it does not take into account the range dependent influence of a joint's dynamics. For this reason, its use should be limited to cases where joints are expected to be very nearly rigid. To account for a greater degree of interface relaxation the interval-based metric should be used.

Overcoming the respective limitations of both the gradient and sampling-based strategies (linearity and computational efficiency), the interval-based metric provides a convenient and computationally efficient identification of the response-critical joints in a complex built-up structure. The information gained though its application may be used to focus model refinement towards the connections or joints that will benefit the modelling effort most.

CRediT authorship contribution statement

J.W.R. Meggitt: Conceptualization, Methodology, Validation, Investigation, Writing – original draft, Writing – review & editing.

Declaration of competing interest

The authors declare that they have no known competing financial interests or personal relationships that could have appeared to influence the work reported in this paper.

Appendix A. Conformal mapping

Eq. (45) ((48)) yields the complex interval bounds of an assembly's admittance matrix (response vector), based on an interval relaxation of the nth joint. Its implementation requires first establishing the interval bounds of $\{w_n\}$, defined as per Eq. (44). In what follows we consider Eq. (44) as a conformal map, and propose a simple algorithm to establish said bounds.

The denominator of Eq. (44) represents a complex interval of the form $\{z\} = \{x\} + i\{y\}$, where the real and imaginary intervals are taken to be, $\{x\} = [\underline{x} \quad \infty]$ and $\{y\} = [\underline{y} \quad \infty]$. Taken together, these intervals describe an open rectangular domain in the complex plane that extends from the point $(\underline{x}, \underline{y})$ to infinity, as shown in Fig. A.13a. This domain contains all possible values of the complex number z given the real and imaginary intervals $\{x\}$ and $\{y\}$. We are interested in the mapping of this domain onto that of the complex variable $w = 1/z$. That is, we are interested in the conformal map $f(z) = 1/z$ applied to the open rectangular domain $\{z\}$. In what follows we seek the smallest complex rectangular interval $\{w\} = \{u\} + i\{v\}$, where $\{u\} = [\underline{u} \quad \overline{u}]$ and $\{v\} = [\underline{v} \quad \overline{v}]$, that encloses the domain of $f(z) = 1/z$.

We start by considering the complex relation,

$$w = u + iv = \frac{1}{x + iy}. \tag{A.1}$$

Taking the reciprocal of the above,

$$x + iy = \frac{1}{u + iv} = \frac{u - iv}{u^2 + v^2} \tag{A.2}$$

we obtain expressions for the real and imaginary parts of z with respect to u and v,

$$x = \frac{u}{u^2 + v^2} > \underline{x}, \qquad y = \frac{-v}{u^2 + v^2} > \underline{y} \tag{A.3}$$

where $\underline{x}$ and $\underline{y}$ represent the lower bounds of the intervals $\{x\}$ and $\{y\}$. Assuming $\underline{x} > 0$, rearranging the left-hand inequality above leads to,

$$0 > u^2 + v^2 - \frac{u}{\underline{x}} = \left(u - \frac{1}{2\underline{x}}\right)^2 + (v-0)^2 - \left(\frac{1}{2\underline{x}}\right)^2, \tag{A.4}$$

or equivalently,

$$\left(\frac{1}{2\underline{x}}\right)^2 > \left(u - \frac{1}{2\underline{x}}\right)^2 + (v-0)^2. \tag{A.5}$$

Recalling that a circle of radius r with centre point (h, k), is given by,

$$r^2 = (u-h)^2 + (v-k)^2. \tag{A.6}$$

the conformal map $f(z) = 1/z$ takes the region $x > \underline{x}$ of the complex plane and maps it to a closed circular domain of radius $r = 1/2\underline{x}$ centred at the coordinates $(1/2\underline{x}, 0)$. See for example the blue domain in Fig. A.13. Note that if $\underline{x} < 0$, the above inequality flips, such that,

$$\left(\frac{1}{2\underline{x}}\right)^2 < \left(u - \frac{1}{2\underline{x}}\right)^2 + (v-0)^2. \tag{A.7}$$

In this case, the conformal map $f(z) = 1/z$ takes the region $x > \underline{x}$ and maps it to the open domain surrounding a circle of radius $r = 1/2|\underline{x}|$ centred at the coordinates $(1/2\underline{x}, 0)$ (with $\underline{x} < 0$ this circle is located in the negative real half-plane). See for example the blue domain in Fig. A.14c.

Let us now consider the inequality for y. Following similar steps as above, assuming $\underline{y} > 0$, we arrive at the inequality,

$$0 > u^2 + v^2 + \frac{v}{\underline{y}} = (u-0)^2 + \left(v - \frac{-1}{2\underline{y}}\right)^2 - \left(\frac{1}{2\underline{y}}\right)^2 \tag{A.8}$$

or equivalently,

$$\left(\frac{1}{2\underline{y}}\right)^2 > (u-0)^2 + \left(v - \frac{-1}{2\underline{y}}\right)^2 \tag{A.9}$$

which equally describes a closed circular domain in complex plane with radius $r = 1/2\underline{y}$ centred at the coordinates $(0, -1/2\underline{y})$. See for example the green domain in Fig. A.13. If $\underline{y} < 0$ the above inequality flips, such that,

$$\left(\frac{1}{2\underline{y}}\right)^2 < (u-0)^2 + \left(v - \frac{-1}{2\underline{y}}\right)^2. \tag{A.10}$$

In this case, the conformal map $f(z) = 1/z$ takes the region $y > \underline{y}$ and maps it to the open domain surrounding a circle of radius $r = 1/2|\underline{y}|$ centred at the coordinates $(0, -1/2\underline{y})$ (with $\underline{y} < 0$ this is in the positive imaginary half-plane). See for example the green domain in Fig. A.14d.

The complex map $f(z) = 1/z$ is shown in Fig. A.13 for the two regions $\underline{x} > 0$ and $\underline{y} > 0$. The intersection of $x > \underline{x}$ and $y > \underline{y}$ in the x, y plane describes the domain of possible complex values $z = x + iy$ that satisfy both $x > \underline{x}$ and $y > \underline{y}$. This domain maps to a vesica piscis (i.e. the intersection of two circles) in the u, v plane, as shown in Figs. A.13b and A.14ab, which describes the range of possible values the complex variable $w = 1/(x + iy)$ can take, given the restrictions on x and y. For the case that $\underline{x} < 0$ *or* $\underline{y} < 0$ the domain maps to a more complex region that is the intersection of an open and closed circular region, as shown in Figs. A.14cd.

To adopted an interval-based approach we seek to describe the resulting intersection by means of the smallest enclosing rectangle. To determine the interval bounds of $1 \oslash \{z\}$ we consider the four cases presented in Fig. A.14:

(a) If $0 < \underline{x} < \underline{y}$ then $\overline{v} = \underline{u} = 0$, $\overline{u} = 1/2\underline{y}$, and $\underline{v} < 0$ corresponds to the point of intersection between the two domain's circular boundaries.

(b) If $\underline{x} > \underline{y} > 0$ then $\overline{v} = \underline{u} = 0$, $\underline{v} = -1/2\underline{x}$, and $\overline{u} > 0$ corresponds to the point of intersection between the two domain's circular boundaries.

(c) If $\underline{x} < 0 < \underline{y}$ then $\overline{v} = 0$, $\underline{v} = -1/\underline{y}$, $\overline{u} = 1/2\underline{y}$, and $\underline{u} < 0$ corresponds to the point of intersection between the two domain's circular boundaries if $1/2|\underline{y}| < 1/2|\underline{x}|$, or $-1/2\underline{y}$ otherwise.

(d) If $\underline{y} < 0 < \underline{x}$ then $\underline{u} = 0$, $\overline{u} = 1/\underline{x}$, $\underline{v} = -1/2\underline{x}$, and $\overline{v} > 0$ corresponds to the point of intersection between the two domain's circular boundaries if $1/2|\underline{x}| < 1/2|\underline{y}|$, or $1/2\underline{x}$ otherwise.

In the case that $\underline{x}, \underline{y} < 0$, the domain of z encloses the origin and so the domain of w extends to $\pm\infty$.

An implementation of the above interval computation is summarised in Algorithm 1. Having established the bounds of $\{w_n\}$, as per the outlined procedure, Eq. (45) can be implemented by adopting the interval arithmetic operations detailed in Section 2, and maximum/minimum bounds of the assembly admittance determined.

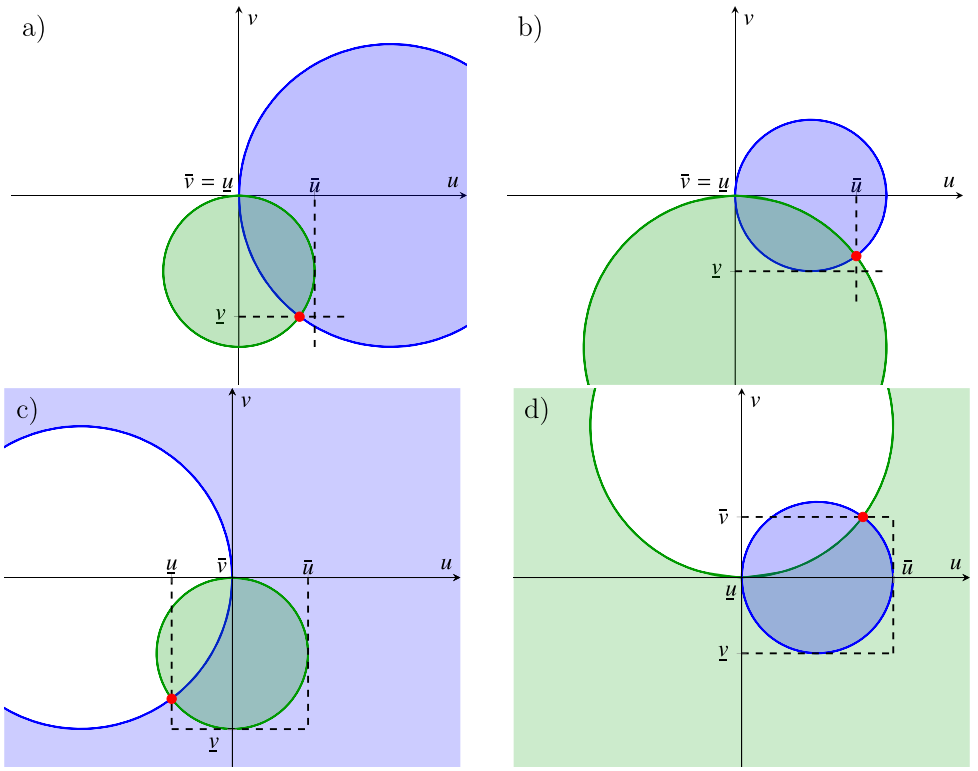

Fig. A.14. Optimum complex interval enclosing $w = 1/(x + iy)$ for $x > \underline{x}$ (blue) and $y > \underline{y}$ (green). Four scenarios are considered: a) $0 < \underline{x} < \underline{y}$, (b) $0 < \underline{y} < \underline{x}$, (c) $\underline{x} < 0 < \underline{y}$, and d) $\underline{y} < 0 < \underline{x}$. (For interpretation of the references to colour in this figure legend, the reader is referred to the web version of this article.)

Appendix B. Intersection point

To determine the intersection point between the boundaries of two circular domains (i.e. the red markers in Fig. A.14) we should solve the following pair of simultaneous equations,

$$(u-u_1)^2 + (v-v_1)^2 = r_1^2, \qquad (u-u_2)^2 + (v-v_2)^2 = r_2^2 \tag{B.1}$$

each representing a circle in the u, v plane. We take subscript 1 to denote the mapped $x > \underline{x}$ domain (blue), and subscript 2 the mapped $y > \underline{y}$ domain (green).

Subtracting Eq. (B.1) from one another yields,

$$-2u(u_1-u_2) - 2v(v_1-v_2) = (r_1^2 - r_2^2) - (u_1^2 - u_2^2) - (v_1^2 - v_2^2) \tag{B.2}$$

Isolating v, whilst noting that for all cases $u_2 = 0$ and $v_1 = 0$, yields,

$$v = -\frac{1}{2}(v_1 - v_2)^{-1}\left((r_1^2 - r_2^2) - (u_1^2 - u_2^2) - (v_1^2 - v_2^2) + 2u(u_1 - u_2)\right) = \frac{1}{2v_2}\left((r_1^2 - r_2^2) - (u_1^2) + (v_2^2) + 2uu_1\right). \tag{B.3}$$

Further, noting that $u_1^2 = r_1^2$ and $v_2^2 = r_2^2$ we have that,

$$v = \frac{1}{2v_2}\left((r_1^2 - r_2^2) - (r_1^2) + (r_2^2) + 2uu_1\right) = \frac{u_1 u}{v_2}. \tag{B.4}$$

Substituting the above into equation ((B.1)a) we get,

$$(u-u_1)^2 + \left(\frac{u_1 u}{v_2}\right)^2 = u_1^2 \tag{B.5}$$

which, after expanding the above and grouping terms, yields a quadratic equation in u,

$$u^2\left(1 + \left(\frac{u_1}{v_2}\right)^2\right) - 2uu_1 = 0, \qquad u = \frac{2u_1 \pm \sqrt{4u_1^2}}{2\left(1 + \left(\frac{u_1}{v_2}\right)^2\right)} = \frac{u_1 \pm u_1}{1 + \left(\frac{u_1}{v_2}\right)^2}. \tag{B.6}$$

Algorithm 1: Determine bounds of the complex interval $\{w\} = [\underline{u} \quad \overline{u}] + i\,[\underline{v} \quad \overline{v}] = \left([\underline{x} \quad \infty] + i\,[\underline{y} \quad \infty]\right)^{-1}$

$r_1 = 1/(2|\underline{x}|)$;
$r_2 = 1/(2|\underline{y}|)$;
if $\underline{x} > 0 \wedge \underline{y} > 0$ **then**
  if $r_2 \le r_1$ **then**
    // this is the case of figure A.14a
    $\underline{u} = 0$;
    $\overline{u} = r_1$;
    $\underline{v} = -2r_1^2/\left(r_2\left(1 + (r_1/r_2)^2\right)\right)$;
    $\overline{v} = 0$;
  else
    // this is the case of figure A.14b
    $\underline{u} = 0$;
    $\overline{u} = 2r_1/\left(1 + (r_1/r_2)^2\right)$;
    $\underline{v} = -r_2$;
    $\overline{v} = 0$;
  end
else if $\underline{x} < 0 \wedge \underline{y} > 0$ **then**
  // this is the case of figure A.14c
  if $r_2 \le r_1$ **then**
    $\underline{u} = 2r_1/\left(1 + (r_1/r_2)^2\right)$
  else
    $\underline{u} = -r_2$
  end
  $\overline{u} = r_2$;
  $\underline{v} = -2r_2$;
  $\overline{v} = 0$;
else if $\underline{y} < 0 \wedge \underline{x} > 0$ **then**
  // this is the case of figure A.14d
  $\underline{u} = 0$;
  $\overline{u} = 2r_1$;
  $\underline{v} = -r_1$;
  if $r_2 \le r_1$ **then**
    $\overline{v} = -2r_1/\left(1 + (r_1/r_2)^2\right)$
  else
    $\overline{v} = r_1$
  end
else
  $\underline{u} = -\infty$;
  $\overline{u} = \infty$;
  $\underline{v} = -\infty$;
  $\overline{v} = \infty$;
end

Taking the positive square-root leads to the following pair of equations for the intersection point,

$$u = \frac{2u_1}{1 + \left(\frac{u_1}{v_2}\right)^2}, \qquad v = -\frac{2u_1^2}{v_2\left(1 + \left(\frac{u_1}{v_2}\right)^2\right)}. \tag{B.7}$$

References

[1] D. De Klerk, D.J. Rixen, S.N. Voormeeren, General framework for dynamic substructuring: History, review, and classification of techniques, AIAA J. 46 (5) (2008) 1169–1181.
[2] M.R.W. Brake, in: M. Brake (Ed.), The Mechanics of Jointed Structures, Springer, 2018.
[3] R.A. Ibrahim, C.L. Pettit, Uncertainties and dynamic problems of bolted joints and other fasteners, J. Sound Vib. 279 (3–5) (2005) 857–936.

[4] D.J. Segalman, Modelling joint friction in structural dynamics, Struct. Control Health Monit. 13 (1) (2006) 430–453.
[5] F. Marques, P. Flores, J.C.P. Claro, H.M. Lankarani, A survey and comparison of several friction force models for dynamic analysis of multibody mechanical systems, Nonlinear Dynam. 86 (3) (2016) 1407–1443.
[6] Y. Ren, C.F. Beards, Identification of joint properties of a structure using FRF data, J. Sound Vib. 186 (4) (1995) 567–587.
[7] Y. Ren, C.F. Beards, Identification of 'effective' linear joints using coupling and joint identification techniques, Trans. ASME. J. Vib. Acoust. 120 (2) (1998) 331–338.
[8] S. Noll, J.T. Dreyer, R. Singh, Identification of dynamic stiffness matrices of elastomeric joints using direct and inverse methods, Mech. Syst. Signal Process. 39 (1–2) (2013) 227–244.
[9] Ş. Tol, H.N. Özgüven, Dynamic characterization of bolted joints using FRF decoupling and optimization, Mech. Syst. Signal Process. 54 (2015) 124–138.
[10] D.R. Roettgen, M.S. Allen, Nonlinear characterization of a bolted, industrial structure using a modal framework, Mech. Syst. Signal Process. 84 (2017) 152–170.
[11] R. de Oliveira Teloli, L.G.G. Villani, S. da Silva, M.D. Todd, On the use of the GP-NARX model for predicting hysteresis effects of bolted joint structures, Mech. Syst. Signal Process. 159 (2021) 107751.
[12] D. Čelič, M. Boltežar, Identification of the dynamic properties of joints using frequency-response functions, J. Sound Vib. 317 (1–2) (2008) 158–174.
[13] Z. Saeed, S.W.B. Klaassen, C.M. Firrone, T.M. Berruti, D.J. Rixen, Experimental joint identification using system equivalent model mixing in a bladed disk, J. Vib. Acoust. 142 (5) (2020) 1–12.
[14] Z. Saeed, C.M. Firrone, T.M. Berruti, Joint identification through hybrid models improved by correlations, J. Sound Vib. Preprint (2020) 1–41.
[15] J.E. Mottershead, M.I. Friswell, G.H. Ng, J.A. Brandon, Geometric parameters for finite element model updating of joints and constraints, Mech. Syst. Signal Process. 10 (2) (1996) 171–182.
[16] F. Gant, P. Rouch, F. Louf, L. Champaney, Definition and updating of simplified models of joint stiffness, Int. J. Solids Struct. 48 (5) (2011) 775–784.
[17] J. Kim, J.C. Yoon, B.S. Kang, Finite element analysis and modeling of structure with bolted joints, Appl. Math. Model. 31 (5) (2007) 895–911.
[18] S. Bograd, P. Reuss, A. Schmidt, L. Gaul, M. Mayer, Modeling the dynamics of mechanical joints, Mech. Syst. Signal Process. 25 (8) (2011) 2801–2826.
[19] S.S. Rao, L. Berke, Analysis of uncertain structural systems using interval analysis, AIAA J. 35 (4) (1997) 727–735.
[20] D. Moens, D. Vandepitte, An interval finite element approach for the calculation of envelope frequency response functions, Internat. J. Numer. Methods Engrg. 61 (14) (2004) 2480–2507.
[21] G. Muscolino, R. Santoro, A. Sofi, Explicit frequency response functions of discretized structures with uncertain parameters, Comput. Struct. 133 (2014) 64–78.
[22] M. Łasecka-Plura, R. Lewandowski, Dynamic characteristics and frequency response function for frame with dampers with uncertain design parameters, Mech. Based Des. Struct. Mach. 45 (3) (2017) 296–312.
[23] W. Lei, L. Yaru, L. Yisi, An inverse method for distributed dynamic load identification of structures with interval uncertainties, Adv. Eng. Softw. 131 (January) (2019) 77–89.
[24] M. Imholz, M. Faes, D. Vandepitte, D. Moens, Robust uncertainty quantification in structural dynamics under scarse experimental modal data: A Bayesian-interval approach, J. Sound Vib. 467 (2020) 114983.
[25] M.Y. Zhao, W.J. Yan, K.V. Yuen, M. Beer, Non-probabilistic uncertainty quantification for dynamic characterization functions using complex ratio interval arithmetic operation of multidimensional parallelepiped model, Mech. Syst. Signal Process. 156 (2021) 107559.
[26] Y. Ben-Haim, I. Elishakoff, Convex Models of Uncertainty in Applied Mechanics, Elsevier, 2013.
[27] L. Chen, S.S. Rao, Fuzzy finite-element approach for the vibration analysis of imprecisely-defined systems, Finite Elem. Anal. Des. 27 (1) (1997) 69–83.
[28] H. Yin, D. Yu, S. Yin, B. Xia, Fuzzy interval Finite Element/Statistical Energy Analysis for mid-frequency analysis of built-up systems with mixed fuzzy and interval parameters, J. Sound Vib. 380 (2016) 192–212.
[29] S.H. Chen, H.D. Lian, X.W. Yang, Interval eigenvalue analysis for structures with interval parameters, Finite Elem. Anal. Des. 39 (5–6) (2003) 419–431.
[30] S.H. Chen, L. Ma, G.W. Meng, R. Guo, An efficient method for evaluating the natural frequencies of structures with uncertain-but-bounded parameters, Comput. Struct. 87 (9–10) (2009) 582–590.
[31] K. Fujita, I. Takewaki, An efficient methodology for robustness evaluation by advanced interval analysis using updated second-order Taylor series expansion, Eng. Struct. 33 (12) (2011) 3299–3310.
[32] G. Muscolino, A. Sofi, Stochastic analysis of structures with uncertain-but-bounded parameters via improved interval analysis, Probab. Eng. Mech. 28 (2012) 152–163.
[33] G. Muscolino, A. Sofi, Bounds for the stationary stochastic response of truss structures with uncertain-but-bounded parameters, Mech. Syst. Signal Process. 37 (1–2) (2013) 163–181.
[34] A.E. Mahmoudi, A.J. Rixen, C.H. Meyer, Comparison of different approaches to include connection elements into frequency-based substructuring, Exp. Tech. 44 (4) (2020) 425–433.
[35] R.S. Langley, Unified approach to probabilistic and possibilistic analysis, J. Eng. Mech. 126 (November) (2000) 1163–1172.
[36] M. Faes, D. Moens, Recent Trends in the Modeling and Quantification of Non-Probabilistic Uncertainty, vol. 27, (3) Springer Netherlands, 2020, pp. 633–671.
[37] M.S. Petkovic, P.D. Ljiljana, Complex Interval Arithmetic and Its Applications, WILEY-VCH, 1998.
[38] S.M. Rump, INTLAB — INTerval LABoratory, Dev. Reliab. Comput. (1999) 77–104.
[39] J. Rokne, P. Lancaster, Complex interval arithmetic, Commun. ACM 14 (2) (1971) 111–112.
[40] R. Lohner, J.W.V. Gudenberg, Complex interval division with maximum accuracy, Proc. - Symp. Comput. Arith. (1985) 332–336.
[41] E.M.N. Mahmood, G. Soylu, An effective method for division of rectangular intervals, AIMS Math. 5 (6) (2020) 6355–6372.
[42] M.S. Allen, D.J. Rixen, M. van der Seijs, P. Tiso, T. Abrahamsson, R.L. Mayes, Substructuring in Engineering Dynamics, Springer International Publishing, 2019.
[43] M. Petyt, Introduction to Finite Element Vibration Analysis, second ed., Cambridge University Press, New York, 2010.
[44] W.W. Hager, Updating the inverse of a matrix, SIAM Rev. 31 (2) (1989) 221–239.
[45] A.T. Moorhouse, A.S. Elliott, T.A. Evans, In situ measurement of the blocked force of structure-borne sound sources, J. Sound Vib. 325 (4–5) (2009) 679–685.
[46] International Organization for Standardization, ISO 20270:2019 ACoustics - Characterization of sources of structure-Borne sound and vibration - Indirect measurement of blocked forces, 2019.
[47] A.S. Elliott, A.T. Moorhouse, T. Huntley, S. Tate, In-situ source path contribution analysis of structure borne road noise, J. Sound Vib. 332 (24) (2013) 6276–6295.
[48] D. Lennström, M. Olsson, F. Wullens, A. Nykänen, Validation of the blocked force method for various boundary conditions for automotive source characterization, Appl. Acoust. 102 (JANUARY) (2016) 108–119.
[49] A.S. Elliott, A.T. Moorhouse, N. Sanei, M. Glesser, J. Sapena, S. Ferella, Structure borne noise characterization of an air generation and treatment unit (AGTU) for a train using the mobility method and sub-structuring, in: INTER-NOISE 2019 MADRID - 48th International Congress and Exhibition on Noise Control Engineering, 2019.
[50] N. Sanei, M. Glesser, J. Sapena, S. Ferella, A.S. Elliott, Structure borne noise characterization of an air generation and treatment unit (AGTU) for a train by using blocked forces method, in: INTER-NOISE 2019 MADRID - 48th International Congress and Exhibition on Noise Control Engineering, 2019.

[51] F. Cabaret, A.S. Elliott, O. Farrell, K. Samami, A.T. Moorhouse, Prediction of structure borne noise and vibration for resiliently coupled equipment using blocked forces and substructuring, in: Roceedings of ISMA 2018-International Conference on Noise and Vibration Engineering and USD 2018-International Conference on Uncertainty in Structural Dynamics, 2020.
[52] N. Patil, A.S. Elliott, A.T. Moorhouse, A blocked pressure based transfer path analysis (TPA) method to measure the sound insulation path contributions of a partition subjected to an incident airborne field, in: 24th International Congress on Sound and Vibration, ICSV 2017, 2017, pp. 1–8.
[53] A. Saltelli, M. Ratto, T. Andres, F. Campolongo, J. Cariboni, D. Gatelli, M. Saisana, S. Tarantola, Global Sensitivity Analysis: The Primer, Wiley, 2008, p. 452.
[54] J.W.R. Meggitt, A.T. Moorhouse, K. Wienen, M. Sturm, A framework for the propagation of uncertainty in transfer path analysis, J. Sound Vib. (2020) 115425.
[55] I.M. Sobol, Global sensitivity indices for nonlinear mathematical models and their Monte Carlo estimates, Math. Comput. Simulation 55 (2001) 271–280.
[56] A. Hjørungnes, Complex-Valued Matrix Derivatives, first ed., vol. 369, (1) Cambrudge University Press, New York, 2013, pp. 1689–1699.
[57] A. Saltelli, P. Annoni, I. Azzini, F. Campolongo, M. Ratto, S. Tarantola, Variance based sensitivity analysis of model output. Design and estimator for the total sensitivity index, Comput. Phys. Comm. 181 (2) (2010) 259–270.
[58] D. Moens, D. Vandepitte, Interval sensitivity theory and its application to frequency response envelope analysis of uncertain structures, Comput. Methods Appl. Mech. Engrg. 196 (21–24) (2007) 2486–2496.
[59] Mathworks, Partial differential equation toolbox ™ user's guide, 2021.
[60] A.S. Elliott, A.T. Moorhouse, G. Pavić, Moment excitation and the measurement of moment mobilities, J. Sound Vib. 331 (11) (2012) 2499–2519.